Journal Pre-proof

Substituted 4-phenylthiazoles: Development of potent and selective A_1, A_3 and dual A_1/A_3 adenosine receptor antagonists

Aliaa Abdelrahman, Swapnil G. Yerande, Vigneshwaran Namasivayam, Tim A. Klapschinski, Mohamad Wessam Alnouri, Ali El-Tayeb, Christa E. Müller

PII: S0223-5234(19)31031-1

DOI: https://doi.org/10.1016/j.ejmech.2019.111879

Reference: EJMECH 111879

To appear in: *European Journal of Medicinal Chemistry*

Received Date: 30 July 2019

Revised Date: 10 November 2019

Accepted Date: 11 November 2019

Please cite this article as: A. Abdelrahman, S.G. Yerande, V. Namasivayam, T.A. Klapschinski, M.W. Alnouri, A. El-Tayeb, C.E. Müller, Substituted 4-phenylthiazoles: Development of potent and selective A_1, A_3 and dual A_1/A_3 adenosine receptor antagonists, *European Journal of Medicinal Chemistry* (2019), doi: https://doi.org/10.1016/j.ejmech.2019.111879.

Substituted 4-phenylthiazoles: development of potent and selective A_1, A_3 and dual A_1/A_3 adenosine receptor antagonists

Aliaa Abdelrahman,[a,b,&] *Swapnil G. Yerande,*[c,d,&] *Vigneshwaran Namasivayam,* [a,b] *Tim A. Klapschinski,* [a,b] *Mohamad Wessam Alnouri,*[a] *Ali El-Tayeb,*[a,b] *and Christa E. Müller*[a,b,]*

[a]Pharmaceutical Institute, Department of Pharmaceutical & Medicinal Chemistry, University of Bonn, An der Immenburg 4, D-53121 Bonn, Germany.

[b]Pharma Center Bonn, University of Bonn, Brühlerstr. 7, D-53121 Bonn, Germany

[c]Department of Medicinal Chemistry, B. V. Patel Pharmaceutical Education and Research Development (PERD) Centre, Ahmedabad 380 054, Gujarat, India.

[d]*present address*: Deepak Nitrite Ltd., Vadodara, Gujarat, India

[&]Authors contributed equally

christa.mueller@uni-bonn.de

*Address correspondence to:

Prof. Dr. Christa Müller

Pharmazeutisches Institut

Pharmazeutische & Medizinische Chemie

An der Immenburg 4, D-53121 Bonn, Germany

Phone: +49-228-73-2301; Fax: +49-228-73-2567

Abstract

Adenosine acts as a powerful signaling molecule via four distinct G protein-coupled receptors, designated A_1, A_{2A}, A_{2B} and A_3 adenosine receptors (ARs). A_{2A} and A_{2B} ARs are G_s-coupled, while A_1 and A_3 ARs inhibit cAMP production via G_i proteins. Antagonists for A_1 and A_3 ARs may be useful for the treatment of (neuro)inflammatory diseases including acute kidney injury and kidney failure, pulmonary diseases, and Alzheimer's disease. In the present study, we optimized the versatile 2-amino-4-phenylthiazole scaffold by introducing substituents at N2 and C5 to obtain A_1 and A_3 AR antagonists including dual-target compounds. Selective A_1 antagonists with (sub)nanomolar potency were produced, e.g. **11** and **13**. These compounds showed species differences being significantly more potent at the rat as compared to the human A_1 AR, and were characterized as inverse agonists. Several potent and selective A_3 AR antagonists, e.g. **7**, **8**, **17** and **22** (K_i values of 5-9 nM at the human A_3 AR) were prepared, which were much less potent at the rat orthologue. Moreover, dual A_1/A_3 antagonists (**10**, **18**) were developed showing K_i values between 8-42 nM. Docking and molecule dynamic simulation studies using the crystal structure of the A_1 AR and a homology model of the A_3 AR were performed to rationalize the observed structure-activity relationships.

Keywords

Adenosine receptors; A_1 adenosine receptor; A_3 adenosine receptor antagonist; allosteric modulator; Alzheimer's disease; inverse agonist; multi-target drugs; selectivity; species differences; structure-activity relationships; synthesis; thiazole

Abbreviations

ADA, adenosine deaminase; AR, adenosine receptor(s); BSA, bovine serum albumin; CADO, 2-chloroadenosine; [^{3}H]CCPA, [^{3}H]2-chloro-*N*^{6}-cyclopentyladenosine; CHO, Chinese

hamster ovary; CPA, N^6-cyclopentyladenosine; cyclic adenosine monophosphate (cAMP); DMSO, dimethylsulfoxide; DPCPX, 8-cyclopentyl-1,3-dipropylxanthine; GTP, guanosine-5'-triphosphate; h, human; m, mouse; [^{3}H]MSX-2, [^{3}H](*E*)-3-(3-hydroxypropyl)-8-(2-(3-methoxyphenyl)vinyl)-7-methyl-1-prop-2-ynyl-3,7-dihydropurine-2,6-dione, NECA, 5'-(*N*-ethylcarboxamido)adenosine; *R*-PIA, (*R*)-N^6-phenylisopropyladenosine; PSA, polar surface area; [^{3}H]PSB-11, [^{3}H]2-phenyl-8-ethyl-4-methyl-(8*R*)-4,5,7,8-tetrahydro-1*H*-imidazo[2.1-*i*]purin-5-one; [^{3}H]PSB-603, [^{3}H]8-(4-(4-(4-chlorophenyl)piperazine-1-sulfonyl)phenyl)-1-propylxanthine; r, rat; TRIS, tris(hydroxy-methyl)aminomethane.

Introduction

Extracellular adenosine acts at G protein-coupled cell membrane receptors (GPCRs), the so-called purine P1 or adenosine receptors (ARs), which are divided into four subtypes: A_1, A_{2A}, A_{2B} and A_3 [1]. A_1 and A_3 ARs are coupled to $G_{i/o}$ proteins which mediate inhibition of adenylate cyclase thereby reducing cAMP production, while A_{2A} and A_{2B} ARs stimulate the production of cAMP via G_s proteins [1, 2]. A_{2B} ARs can be additionally coupled to G_q proteins leading to phospholipase C activation and subsequent calcium mobilization [3]. ARs are widely distributed in the body, and elevated adenosine levels and/or receptor upregulation have been observed under many pathological conditions [4]. The A_1 AR is found in high density in the brain, in cortex, hippocampus, and cerebellum, mediating neurotransmitter release from neurons; moreover, it is expressed on astrocytes, oligodendrocytes, and microglia [5]. In the periphery, A_1 ARs are present in many organs and tissues including heart and kidneys [6]. A_3 ARs have been detected in various organs such as lung and liver [7]; in addition, they are expressed on immune cells and on various cancer cells [7,8].

Both, A_1 and A_3 AR antagonists, may be useful and might even show synergistic effects for the treatment of important diseases including (i) acute kidney injury and kidney failure [2],

(ii) inflammatory pulmonary disease, asthma and allergy [9], and (iii) Alzheimer's disease [10-12]. Importantly, both receptors target the same, G_i-mediated pathway.

There is recent evidence that A_1 AR antagonists reduce tau aggregation [10], while A_3 AR antagonists protect from amyloid generation [11]. A_1 antagonists are known to improve cognition, and both, A_1 and A_3 antagonists were found to exert neuroprotective properties in preclinical studies [12].

Selective A_1 and A_3 AR antagonists have been developed, and selective A_1 AR antagonists were clinically evaluated [13]. A phase III clinical trial of the selective A_1 antagonist rolofylline for the treatment of congestive heart failure had shown excellent tolerability of the drug, but lack of efficacy [14]. A recent stratified re-evaluation of the data showed that rolofylline could be harmful in low-risk acute heart failure patients, while it might be significantly beneficial for higher risk patients [15]. A_1 ARs antagonists may be useful for the treatment of cognitive dysfunction, as observed in Alzheimer's disease (AD), due to their CNS stimulatory effects. A recent study indicates that rolofylline is an interesting candidate to combat the hypometabolism and neuronal dysfunction associated with tau-induced neurodegenerative diseases [10].

Selective A_3 AR antagonists have not entered into clinical trials so far. One reason may be the large species differences between human and rodent A_3 ARs. The development of antagonists that are equally potent in both species has so far only met with limited success [2,8,16].

It is known that the treatment of complex diseases requires multifaceted approaches instead of targeting a single pathway [17]. Multi-target drugs are considered safer than drug combinations since they have lower toxicities and a lower risk of drug-drug interactions [18]. Moreover, the combination of several drugs often reduces patient compliance [18]. For these reasons, the development of dual- or multi-target drugs can offer significant advantages [19].

A dual A_{2B}/A_3 AR antagonist was designed as an anti-asthmatic agent [20], while dual A_{2A} agonists/A_3 AR antagonists have been developed for the treatment of asthma and other inflammatory diseases [21,22]. A_1/A_{2A} dual AR antagonists were previously synthesized with the goal to treat neurodegenerative diseases including Parkinson's [23].

No pharmacological data on dual A_1/A_3 AR ligands have been published, but a combination of an A_1 AR agonist with an A_3 AR antagonist was claimed in a patent for the treatment of glaucoma [24]. Recently, we obtained a dual A_1/A_3 AR antagonist, 5-diphenyl[1,2,4]triazolo[1,5-*c*]quinazoline (K_i human A_1 AR 51.6 nM, human A_3 AR 11.1 nM), within a series of antagonists targeted towards the A_{2A} AR [25].

The naturally occurring xanthine derivatives caffeine (I) and theophylline (II) are weak, nonselective AR antagonists (Fig.1) [1,26]. Caffeine (**I**) has been used as a drug for various indications including central stimulation to increase alertness and wakefulness, in combination with analgesics to treat pain, and for the treatment of apnea in premature babies [2,27]. Modification of the xanthine structure, in particular by substitution at the 8-position, has led to derivatives provided with high affinity and subtype-selectivity. For example, PSB-36 (**III**) is one of the most potent A_1 AR antagonists with high affinity for human, rat and mouse ARs, and high selectivity for the A_1 AR against the other AR subtypes [28]. Very recently X-ray structures of the A_1 and the A_{2A} AR in complex with PSB-36 have been published [29]. The 1,3-dipropyl-8-(3-noradamantyl)xanthine, rolofylline (**IV**), is another potent and selective adenosine A_1 AR antagonist [30]. PSB-10 (**Va**) and PSB-11 (**Vb**), see Fig. 1, are tricyclic xanthine derivatives, that show high affinity and selectivity for the human A_3 AR [31]. The pyridine derivative MRS1523 (**VI**) was the first A_3 AR antagonist that displayed considerable potency of the rat A_3 AR [32].

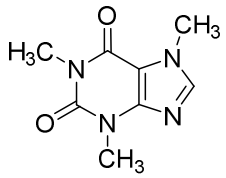

I Caffeine (non-selective)
hA_1 (K_i) = 10,700 nM [26], rA_1 (K_i) = 41,000 nM [26]
hA_{2A} (K_i) = 23,400 nM [26], rA_{2A} (K_i) = 45,000 nM [26]
hA_{2B} (K_i) = 33,800 nM [26], rA_{2B} (K_i) = 30,000 nM [26]
hA_3 (K_i) = 13,300 nM [26], rA_3 (K_i) > 100,000 nM [26]

II Theophylline (non-selective)
hA_1 (K_i) = 6,770 nM [26], rA_1 (K_i) = 14,000 nM [26]
hA_{2A} (K_i) = 1,710 nM [26], rA_{2A} (K_i) = 22,000 nM [26]
hA_{2B} (K_i) = 9,070 nM [26], rA_{2B} (K_i) = 15,100 nM [26]
hA_3 (K_i) = 22,300 nM [26], rA_3 (K_i) > 100,000 nM [26]

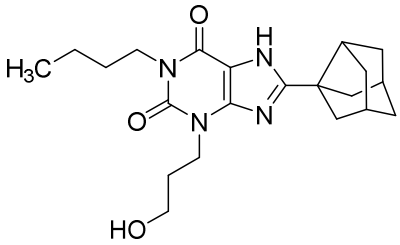

III PSB-36 (A_1-selective)
hA_1 (K_i) = 0.700 nM [26], rA_1 (K_i) = 0.124 nM [26]
hA_{2A} (K_i) = 980 nM [26], rA_{2A} (K_i) = 552 nM [26]
hA_{2B} (K_i) = 187 nM [26], rA_{2B} (K_i) = 350 nM [26]
hA_3 (K_i) = 2,300 nM [26], rA_3 (K_i) = 6,500 nM [26]

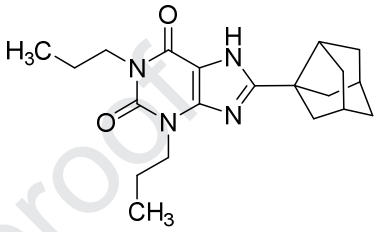

IV Rolofylline (A_1-selective)
hA_1 (K_i) = 0.700 nM [26], rA_1 (K_i) = 0.190 nM [26]
hA_{2A} (K_i) = 108 nM [26], rA_{2A} (K_i) = 380 nM [26]
hA_{2B} (K_i) = 296 nM [26]
hA_3 (K_i) = 4,390 nM [26]

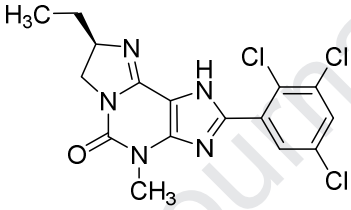

Va PSB-10 (A_3-selective)
hA_1 (K_i) = 1,700 nM [26], rA_1 (K_i) = 805 nM [26]
hA_{2A} (K_i) =2,700 nM [26], rA_{2A} (K_i) =6,040 nM [26]
hA_{2B} (K_i) = 30,000 nM [26]
hA_3 (K_i) = 0.441 nM [26]

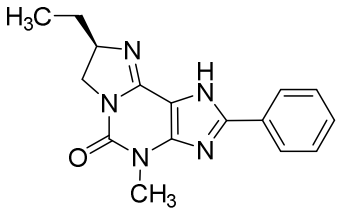

Vb PSB-11 (A_3-selective)
hA_1 (K_i) = 1,640 nM [26], rA_1 (K_i) = 440 nM [26]
hA_{2A} (K_i) =1,280 nM [26], rA_{2A} (K_i) =2,100 nM [26]
hA_{2B} (K_i) = 3,700 nM [26]
hA_3 (K_i) = 2.34 nM [26], rA_3 (K_i) > 10,000 [26]

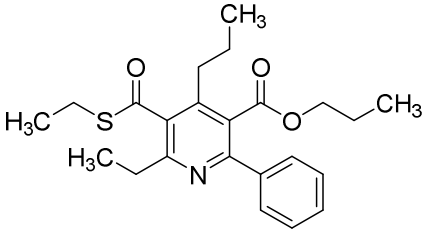

VI MRS1523 (A_3-selective)
hA_1 (K_i) >10,000 [26], rA_1 (K_i) =15,600 nM [32]
hA_{2A} (K_i) = 3,660 nM [26], rA_{2A} (K_i) =2,100 nM [32]
hA_{2B} (K_i) > 10,000 nM [26], rA_{2B} (K_i) > 10,000 nM [30]
hA_3 (K_i) = 18.9 nM [3], rA_3 (K_i) = 113 nM [32]

Fig. 1. Structures and affinities of selected AR antagonists. (h = human, r = rat)

Thiazole derivatives, such as 7-imino-2-thioxothiazolo[4,5-*d*]pyrimidines (e.g. **VII**), related thiazolotriazolopyrimidinethiones (e.g., **VIII**) and 4-benzylideneamino-2,3-dihydro-2-thioxothiazole-5-carbonitrile derivatives, e.g. compound **IX** (Fig. 2), have been reported as potent A_{2A}-selective AR antagonists [33-35]. The benzothiazole derivative tozadenant (SYN-115, **X**) was developed as a potent and selective A_{2A} AR antagonist, and evaluated in phase III clinical trial for the treatment of Parkinson's disease, but has been discontinued due to toxicity [2,36]. We previously showed that substitution of the 2-amino-4-phenylthiazole scaffold with a benzoyl moiety at the amino group and an aroyl moiety at the 5-position shifted the selectivity profile towards the A_1 AR; the most potent compound in this series was **XI** (Fig. 2) [37]. Recently, furanoylamide derivatives of 4,5-disubstituted 2-aminothiazoles were synthesized as adenosine receptor antagonists, e.g. compound **XII**, which showed a high affinity for ARs in the low nanomolar range but lacked subtype-selectivity (Fig. 2) [38]. Thiazole derivatives were also found to be promising scaffolds for A_3 AR antagonists, for example, compound **XIII** displayed a subnanomolar affinity for the human A_3 AR combined with high selectivity versus the other AR subtypes (Fig. 2) [39-40].

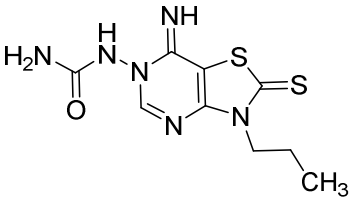

VII (A_{2A}-selective)
hA_1 (K_i) = 2.8 nM [33]
hA_{2A} (K_i) = 0.0038 nM [33]

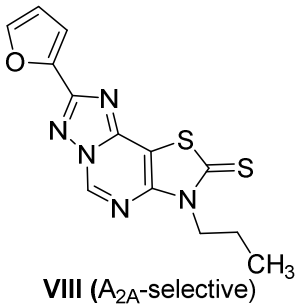

VIII (A_{2A}-selective)
hA_1 (K_i) = 228.4 nM [34]
hA_{2A} (K_i) = 0.38 nM [34]

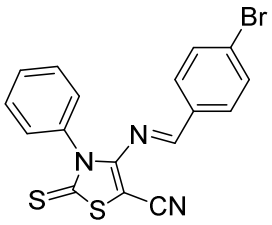

IX (A_{2A}-selective)
hA_1 (K_i) = 186 nM [35]
hA_{2A} (K_i) = 0.0042 nM [35]

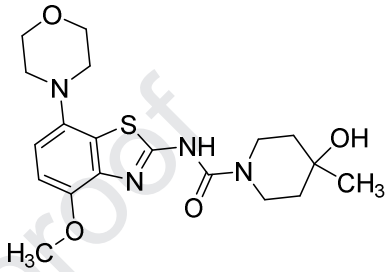

X Tozadenant (A_{2A}-selective)
hA_1 (K_i) = 2,240 nM [36]
hA_{2A} (K_i) = 8.3 nM [36]

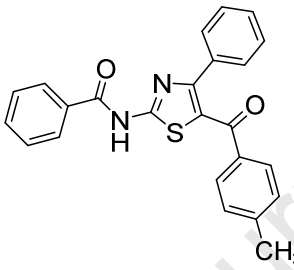

XI (A_1-selective)
hA_1 (K_i) = 57.4 nM34, rA_1 (K_i) = 4.83 nM[37]
hA_{2A} (K_i) = 6,250 nM [37], rA_{2A} (K_i) > 1,000nM[37]
hA_{2B} (K_i) >1,000 nM [37]
hA_3 (K_i) = 2,160 nM [37]

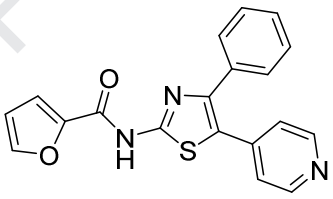

XII (non-selective)
hA_1 (K_i) = 0.580 nM [38]
hA_{2A} (K_i) = 6.65 nM [38]
hA_{2B} (K_i) = 2.78 nM [37]
hA_3 (K_i) = 9.36 nM [37]

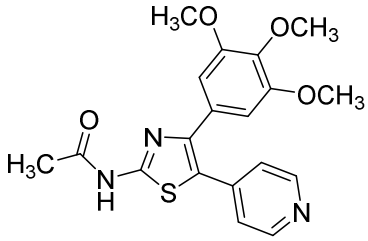

XIII (A_3-selective)
hA_1 (K_i) > 10,000 nM [39]
hA_{2A} (K_i) > 10,000 nM [39]
hA_{2B} (K_B) = 3,200 nM [39]
hA_3 (K_i) = 0.4 nM [39]

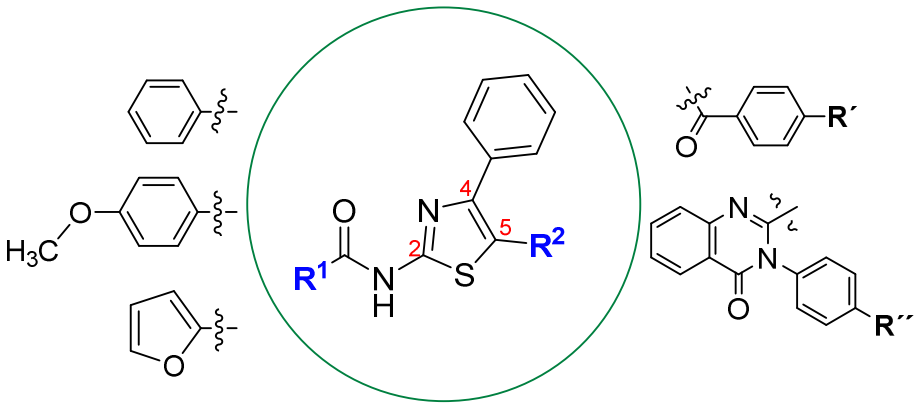

Fig. 2. Structures and affinities of selected thiazole derivatives as AR antagonists and general structures of the designed compounds.

In the present study, we optimized the versatile 2-amino-4-phenylthiazole scaffold by various modifications at the amino group and at the 5-position (for structures of the new compounds see Fig. 2). Our goal was to obtain antagonists with high affinity for A_1 and/or A_3 ARs, preferably acting as dual-target drugs, due to their therapeutic potential for the treatment of kidney failure, inflammatory pulmonary diseases, and Alzheimer's disease.

Results and Discussion

Chemistry

Thiazole derivatives were prepared as described in Scheme 1. 4-Methoxybenzoyl chloride (**1b**), benzoyl chloride (**1a**), or furan-2-carbonyl chloride (**1c**) were reacted with ammonium thiocyanate in acetone to afford the intermediate isothiocyanates [41], which were treated with *N*,*N*-diethylbenzimidamide in acetone to give **2a-c** (Scheme 1) in good yields (65-80%) [42]. *N*,*N*-Diethylbenzimidamide was obtained by reaction of benzonitrile with diethylamine in the presence of aluminium chloride as previously described [43] (for details see Supporting Information (SI)). 2-Chloromethylquinazoline-4-one derivatives used for the synthesis of thiazoles **6-9**, **15-17** and **20-23** were prepared by reaction of anthranilic acid with chloroacetyl chloride in dichloromethane in the presence of triethylamine yielding 2-(2-chloroacetylamino)benzoic acid in 64% yield [44]. Activation of 2-(2-chloroacetylamino)benzoic acid with phosphorus oxychloride in toluene yielding the acid chlorides followed by cyclization with aniline or its derivatives afforded the desired 2-chloromethylquinazoline-4-ones [43]. Phenacyl bromide derivatives used for the synthesis of thiazoles **3**, **5**, **10-14**, and **18**, **19** were obtained by reaction of the corresponding acetophenones with bromine in glacial acetic acid in the presence of a catalytic amount of

aqueous hydrobromic acid [38]. 2-(Bromomethyl)pyridine employed in the synthesis of thiazole **4** was obtained from commercial sources. Reaction of **2a-c** with the appropriate phenacyl bromide derivatives, 2-chloromethylquinazoline-4-one derivatives, or bromopyridine in acetonitrile or methanol, respectively, led to the formation of thiazole derivatives **3-23** in acceptable to high yields ranging from 28% to 96% (Scheme 1) [38,45].

Scheme 1. Synthesis of thiazole derivatives.[a]

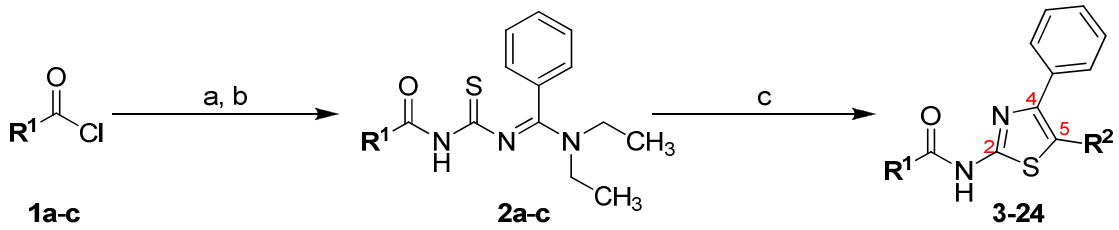

Compound	R^1	R^2
1a, **2a**, **3-9**	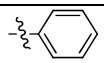	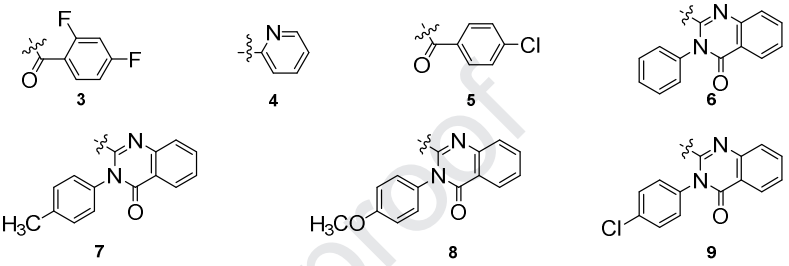
1b, **2b**, **10-17**	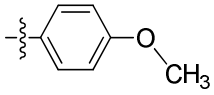	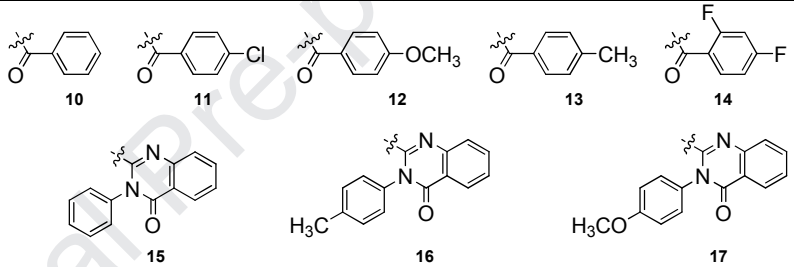
1c, **2c**, **18-23**		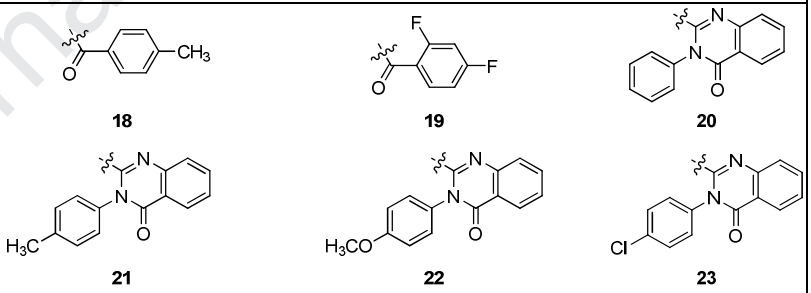

[a]**Reagents, conditions:** (a) NH_4NCS, acetone, reflux, 5 min; (b) *N*,*N*-diethylbenzimidamide, acetone, 0 °C; (c) R^2-CH_2Br, acetonitrile or methanol, rt, 1 h.

Thiazoles **5-10** and **20-23** had previously been described but they had not been biologically evaluated [46]. Those compounds were now resynthesized and investigated. All other synthesized products (**3-4** and **11-19**) are new and not previously described in the literature. Thiazole derivatives **3-23** precipitated from the reaction medium as pure products, and chromatographic purification was therefore not required. The structures of the synthesized

compounds were confirmed by ^{1}H- and ^{13}C-NMR spectroscopy and high resolution mass spectrometry (HRMS). In addition, IR spectra were recorded. Purity of the final compounds was determined by HPLC-ESI-UV/MS analysis and found to be > 95% in all cases (see Experimental Section and SI).

Biological investigations

Receptor-radioligand binding studies at human and rat A_1, A_{2A}, A_{2B} and A_3 ARs were performed as previously described [47-51]. Initially, the 4-phenylthiazoles were tested at a single concentration of 10 µM, 1 µM or 100 nM, respectively, depending on their solubility. For compounds that inhibited radioligand binding by more than 50% full concentration-inhibition curves were recorded and K_i values were determined. All results are collected in Table 1 together with data for standard compound **XI** [37] which we tested in the same test system. For selected compounds, cAMP accumulation assays in Chinese hamster ovary (CHO) cells recombinantly expressing the human A_3 AR were performed (see Fig. 6). Receptor functionality at the A_1 AR was determined by GTP shift assays, in which affinities of selected compounds for the A_1 AR were determined in the absence and presence of 100 µM GTP [37] (see Fig. 7 and Table 2). In addition, affinities for the A_1 AR were determined *vs.* the antagonist radioligand [^{3}H]DPCPX as well as *vs.* the agonist radioligand [^{3}H]CCPA (see Table 3). Agonists will show significantly higher affinity versus an agonist radioligand than versus an antagonist radioligand, while neutral antagonists will display similar affinities versus both, agonist and antagonist radioligands [49]. Antagonists with inverse agonistic activity, on the other hand, will show higher affinity when measured versus an antagonist than versus an agonist radioligand.

Table 1. Affinities of thiazole derivatives at adenosine receptor subtypes.

Compd.	R^2	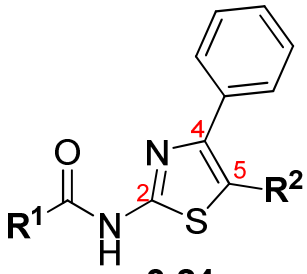 **3-24**			
		K_i ± SEM (nM) at human (h) or rat (r) adenosine receptors (or % inhibition of radioligand binding at indicated concentration)			
		A_1 ***vs.* [^{3}H]CCPA**	**A_{2A}** ***vs.* [^{3}H]MSX-2**	**A_{2B}** ***vs.*[^{3}H]PSB-603**	**A_3** ***vs.*[^{3}H]PSB-11(h) or *vs.*[^{3}H]NECA (r)**
XI [37]	-	**57.4** ± 8.3 (h) **4.83** ± 1.06 (r)	**6250** ± 1970 (h) >1,000 (r)	**>1000** (h)	**2160** ± 880 (h)
Thiazole derivatives 3-9: R^1 = phenyl					
3	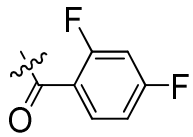	**55.3** ± 22.5 (h)[a] **2.79** ± 0.09 (r)[b]	**77.7** ± 15.6 (h)[c] ≥1000 (43 %) (r)[d]	**>100** (15 %) (h)[a,e]	**67.8** ± 2.7 (h)[a,f]
4	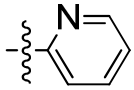	**90.8** ± 2.5 (h)[a] **3.47** ± 0.71 (r)[b]	**83.6** ± 15.5 (h)[c] **391** ± 178 (r)[d]	≥100 (33 %) (h)[a,e]	≥1000 (45 %) (h)[a,f]
5	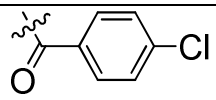	**24.4** ± 4.1 (h)[a] **0.939** ± 0.486 (r)[b]	**39.1** ± 2.4 (h)[c] **1670** ± 550 (r)[b]	>100 (0 %) (h)[a,e]	**428** ± 53 (h)[a,f]
6	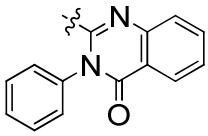	>1000 (0 %) (h)[a] >1000 (1 %) (r)[b]	>1000 (0 %) (h)[c] >1000 (3 %) (r)[d]	>100 (0 %) (h)[a,e]	**111** ± 7 (h)[a,f]
7	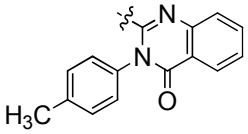	>1000 (0 %) (h) [a] >1000 (23%) (r)[b]	>1000 (0 %) (h)[c] >1000 (17 %) (r)[d]	>100 (0) (h)[a,e]	**9.05** ± 1.20 (h)[a,f] **806** ± 178 (r)[g,h]

8	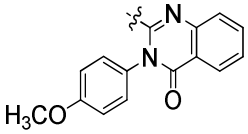	>1000 (6 %) (h)[a] >1000 (10 %) (r)[b]	>1000 (3 %) (h)[c] >1000 (17 %) (r)[d]	>100 (0 %) (h)[a,e]	**8.23** ± 0.89 (h)[a,f] **1320** ± 600 (r)[g,h]
9	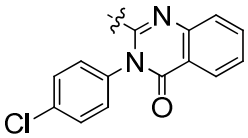	>1000 (4 %) (h)[a] >1000 (16 %) (r)[b]	>1000 (0 %) (h)[c] >1000 (7 %) (r)[d]	>100 (12 %) (h)[a,e]	**83.3** ± 2.5 (h)[a,f] >10000 (r)[g,h] (22 %)
Thiazole derivatives 10-17: R^1 = *p*-methoxyphenyl					
10	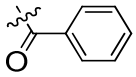	**36.7** ± 5.1 (h)[a] **1.47** ± 0.16 (r)[b]	≥1000 (41 %) (h)[c] ≥1000 (32 %) (r)[d]	>100 (2 %) (h)[a,e]	**25.4** ± 5.2 (h)[a,f] >1,000 (r)[g,h] (0 %)
11	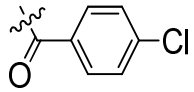	**32.3** ± 8.3 (h)[a,i] **1.01** ± 0.33 (r)[b]	>1000 (0 %) (h)[c] >1000 (12 %) (r)[d]	>100 (0 %) (h)[a,e] >100 (0 %) (r)[j,e]	>1000 (3 ± 4) (h) [a,f] >10000 (0 %) (r)[g,h]
12	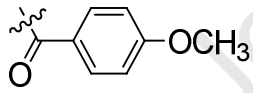	**13.6** ± 4.6 (h)[a] **1.77** ± 0.88 (r)[b]	>1000 (0 %) (h)[c] >1000 (16 %) (r)[d]	>100 (0 %) (h)[a,e]	>1000 (37 %) (h)[a,f]
13	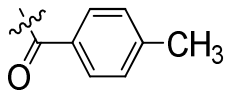	**9.69** ± 4.81 (h)[a] **0.529** ± 0.043 (r)[b]	>1000 (28 %) (h)[c] >1000 (15 %) (r)[d]	>100 (2 %) (h)[a,e] >100 (7 %) (r)[j,e]	≥1000 (45 %) (h)[a,f] >10000 (13 %) (r)[g,h]
14	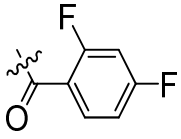	>1000 (9 %) (h)[a] ca. 1000 (54 %) (r)[b]	>1000 (14 %) (h)[c] >1000 (16 %) (r)[d]	>100 (0 %) (h)[a,e]	>1000 (24 %) (h)[a,f]
15	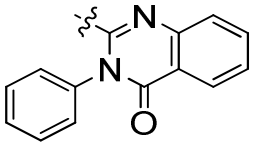	>1000 (0 %) (h)[a] >1000	>1000 (20 %) (h)[c] >1000	>100 (0 ± 17) (h)[a,e]	**174** ± 19 (h)[a,g]

		(11 %) (r)[b]	(1 %) (r)[d]		
16	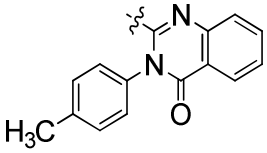	>1000 (0 %) (h)[a] ≥1000 (25 %) (r)[b]	>1000 (0 %) (h)[c] >1000 (15 %) (r)[d]	>100 (2 %) (h)[a,e]	**27.8** ± 8.6 (h)[a,f] >10000 (15 %) (r)[g,h]
17	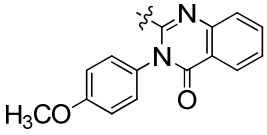	>1000 (3 %) (h)[a] >1000 (17 %) (r)[b]	>1000 (10 %) (h)[c] >1000 (1 %) (r)[d]	>100 (0 %) (h)[a]	**4.63** ± 1.64 (h)[a,f] >10000 (0 %) (r)[g,h]
Thiazole derivatives 18-23: R^1 = 2-Furyl					
18	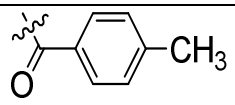	**7.57** ± 0.71 (h)[a] **0.348** ± 0.134 (r)[b]	**1210** ± 709 (r)[d]	>100 (2 %) (h)[a,e]	**42.2** ± 18.5 (h)[a,f]
19	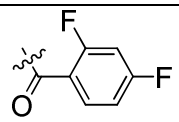	**178** ± 14 (h)[a] **6.69** ± 1.35 (r)[b]	**132** ± 25 (h)[c,h] **73.3** ± 6.6 (r)[d]	>100 (15 %) (h)[a,e]	**124** ± 2 (100 %) (h)[a,f]
20	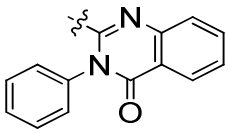	>1000 (1 %) (h)[a] ≥1000 (26 %) (r)[b]	>1000 (5 %) (h)[c] >1000 (33 %) (r)[d]	>100 (1 %) (h)[a,e]	**129** ± 26 (h)[a,f]
21	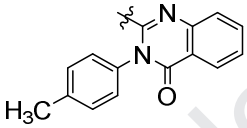	>1000 (2 %) (h)[a] ≥1000 (25 %) (r)[b]	>1000 (1 %) (h)[c] >1000 (6 %) (r)[d]	>100 (0 %) (h)[a]	**25.4** ± 5.3 (h)[a,f] **1840** ± 380 (r)[g,h]
22	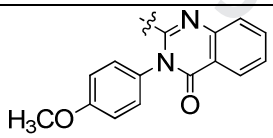	>1000 (7 %) (h)[a] ≥1000 (25 %) (r)[b]	>1000 (11 %) (h)[c] >1000 (0 %) (r)[d]	≥100 (30 %) (h)[a,e]	**6.45** ± 5.34 (h)[a,f] **973** ± 148 (r)[g,h]
23	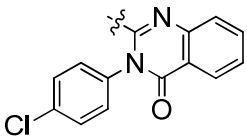	>1000 (0 %) (h)[a] ≥1000 (24 %) (r)[b]	>1000 (8 %) (h)[c] >1000 (14 %) (r)[d]	>100 (1 %) (h)[a,e]	**48.3** ± 2.3 (h)[a,f] **607** ± 48 (r)[g,h]

[a]human recombinant receptors expressed in CHO
[b]A_1: rat brain cortex (for A_1)
[c]human recombinant receptor expressed in HEK293 cells
[d]A_{2A}: rat brain striatum (for A_{2A})
[e]inhibition at 0.1 µM
[f]*vs.*[^{3}H]PSB-11

[g] *vs.* [^{3}H]NECA
[h] rat recombinant receptor expressed in CHO cells
[i] Extrapolated K_i value (due to limited solubility)

Structure-activity relationships

The 2-amino-4-phenylthiazole core structure was modified at the amino group by amide formation with benzoic acid, *p*-methylbenzoic acid, or 2-furancarboxylic acid, respectively. These residues were selected to occupy the lipophilic, aromatic binding pocket. They were combined with different substituents in the 5-position of the 2-amino-4-phenylthiazole core, in particular differently substituted benzoyl residues and a 3-arylquinazolin-4-one moiety. The latter bulky substituent had been found in preliminary studies to confer A_3 AR affinity and selectivity, while the smaller benzoyl substitution appeared to be well tolerated by the A_1 AR. The obtained series of 4-phenylthiazole derivatives **3-23** was investigated in radioligand binding studies at the four human AR subtypes. Our goal was to enhance A_1 and/or A_3 AR affinity, and to obtain antagonists with selectivity for one of both subtypes, as well as dual A_1/A_3 AR antagonists. Test results are displayed in Table 1.

In the present series, the introduction of phenyl (see results of compounds **3-9**), *p*-methoxyphenyl (see results of compounds **10-17**) or furanyl moieties (see results of compounds **18-23**) attached to the amide linker in the 2-position of the thiazole core was generally well tolerated. At the human A_1 AR, higher affinity was obtained with compounds bearing relatively small residues attached to the position 5 of the thiazole core (see $\mathbf{R^1}$ in Scheme 1 and Table 1). At human A_1 ARs several compounds showed high affinity in the low nanomolar concentration range. The 2,4-difluorobenzoyl derivative, compound **3**, and the 2-pyridyl derivative **4** displayed K_i values of 55.3 and 90.8 nM, respectively. The best results in the present series were obtained with benzoyl- (**10**, K_i 36.7 nM), *p*-chlorobenzoyl- (**5**, K_i 24.4 nM; **11**, K_i 32.3 nM), *p*-methoxybenzoyl- (**12**, 13.6 nM), and *p*-methylbenzoyl-substituted thiazole derivatives (**13**, K_i 9.69 nM; **18**, K_i 7.57 nM) (see Table 1), compounds **11**, **12** and **13**

displaying selectivity versus the other AR subtypes (Table 1 and Fig. 3). All tested compounds were weaker at the human A_1 AR as compared to the rat A_1 AR (e.g. **11**: 32-fold, **12**: 8-fold, **13**: 18-fold difference).

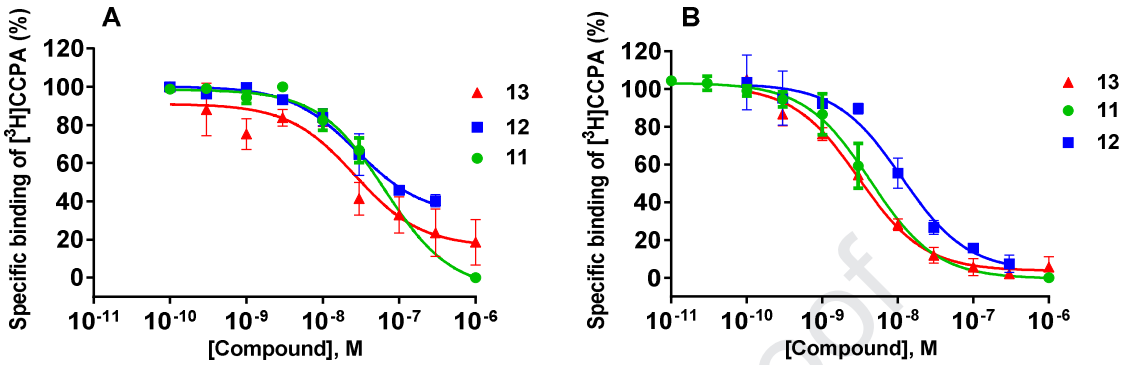

Fig. 3. Concentration-inhibition curves of selected compounds at (**A**) the human A_1 AR recombinantly expressed in CHO cells, and (**B**) at rat cortical membrane preparations; [^{3}H]CCPA (0.5 nM) was used as a radioligand. Data points are means ± SEM of three separate experiments.

In contrast to the human A_1 AR, higher potency for the human A_3 ARs was obtained with compounds bearing bulky residues attached to the 5-position of the thiazole core (see for example compounds **7**, **8**, **17**, **21**, and **22**, see Table 1). These compounds displayed K_i values for the human A_3 AR in the low nanomolar range and were highly selective versus the other AR subtypes. The most potent A_3 AR antagonist at the human receptor was **17** (K_i 4.63 nM) The antagonists exhibited significant species differences between human and rat A_3 ARs. For example, compounds **7**, **21** and **22** showed 72 to 150-fold higher affinities for the human as compared to the rat A_3 AR (Table 1). The 3-(*p*-substituted phenyl)-2-(thiazol-5-yl)quinazolin-4(3*H*)-one moiety appeared to be well tolerated by the rat A_3 AR, e.g. compounds **7** (*p*-methyl), **22** (*p*-methoxy) and **23** (*p*-chloro) showing submicromolar K_i values at the rat A_3 AR. Compound **23** was the most potent antagonist of the present series at the rat A_3 AR (K_i 607 nM), but it was about 13-fold more potent at the human A_3 AR (48.3 nM, see Table 1 and

Fig. 4). In contrast, compounds **10**, **16**, and **17** displayed high affinity for the human A_3 AR in the nanomolar range but no affinity was observed for the rat A_3 AR even at high concentrations.

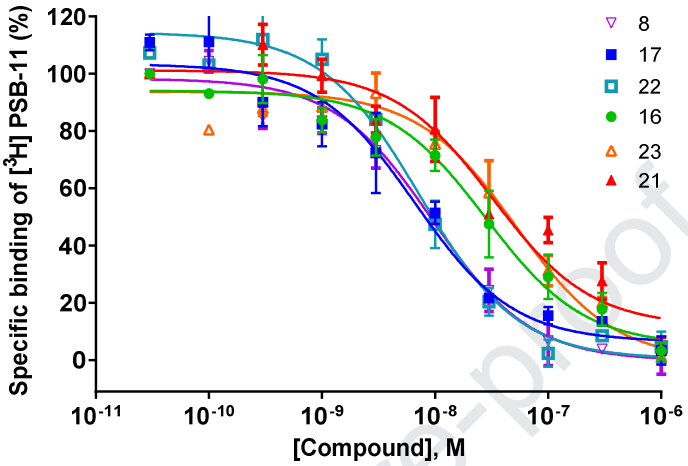

Fig. 4. Concentration-inhibition curves of selected compounds at human A_3 ARs recombinantly expressed in CHO cells. [^{3}H]PSB-11 (0.5 nM) was used as a radioligand. Data points are means ± SEM of three separate experiments.

A combination of 4-methylbenzoyl in position 5 with a furan-2-carboxamide in position 2 of the thiazole core resulting in compound **18** showed the highest dual affinity for the human A_1 and A_3 ARs (K_i A_1 7.57 nM, A_3 42.2 nM). *N*-(5-Benzoyl-4-phenylthiazol-2-yl)-4-methoxybenzamide (**10**) displayed almost identical affinity for the human A_1 AR and the human A_3 AR with K_i values of 36.7 nM and 25.4 nM, respectively. This compound showed no affinity for the other AR subtypes. Both compounds, **10** and **18**, are potent dual A_1/A_3 AR antagonists (see Fig. 5 and Table 1).

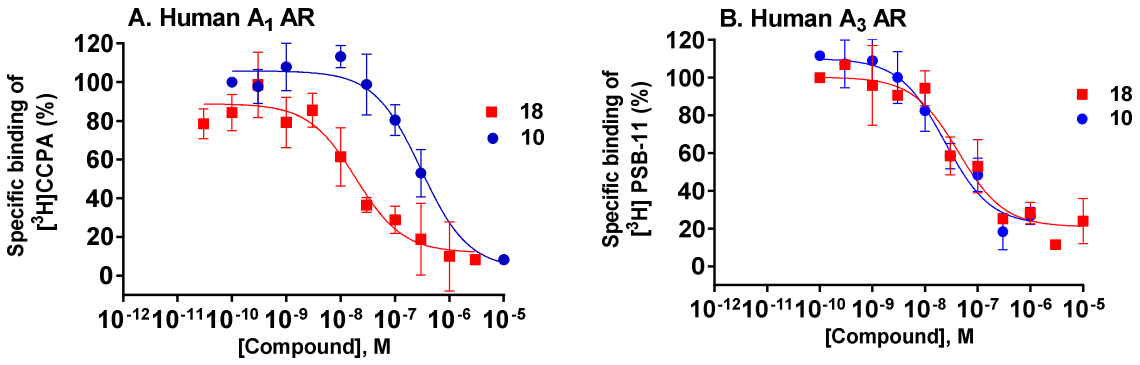

Fig. 5. Concentration-inhibition curves of compounds **10** and **18** tested at (**A**) the human A_1 AR recombinantly expressed in CHO cells *vs.* [^{3}H]CCPA (0.5 nM), and (**B**) the human A_3AR recombinantly expressed in CHO cells *vs.* [^{3}H]PSB-11 (0.5 nM). Data points represent means ± SEM from three separate experiments.

In the studied series only *N*-(5-(2,4-difluorobenzoyl)-4-phenylthiazol-2-yl)-4-methoxybenzamide (**14**) was inactive at all four AR subtypes. Out of the 21 tested compounds four showed affinity for the human A_{2A} AR with K_i values ranging between 39.1 and 132 nM (compounds **3**, **4**, **5** and **19**). All other tested compounds were inactive at concentrations up to 1 µM. At the rat A_{2A} ARs, the compounds showed even lower potency. Only compound **4** exhibited a measurable K_i value of 391 nM at the rat A_{2A} AR (Table 1). All tested compounds were inactive at the human A_{2B} AR. Selected compounds **11** and **13** tested at the rat A_{2B} AR also showed no affinity at that receptor.

cAMP accumulation assays

In order to confirm that the compounds are antagonists, we investigated compound **23** in cAMP accumulation assays at A_3 ARs. A concentration-dependent inhibition curve for the agonist NECA was determined in the absence and in the presence of **23** at rat A_3 ARs expressed in CHO cells. Compound **23** (3 µM and 10 µM) shifted of the concentration-

response curve of the agonist NECA to the right. Thus, **23** can be considered as a competitive A_3 AR antagonist.

The EC_{50} values for the agonist NECA were 5.28 nM without agonist, and 56.9 nM and 1720 nM, respectively, in the presence of 3 µM and 10 µM of **23** (Fig. 6). The calculated K_B value for compound **23** was 314 nM and thus similar to its K_i value determined in binding studies.

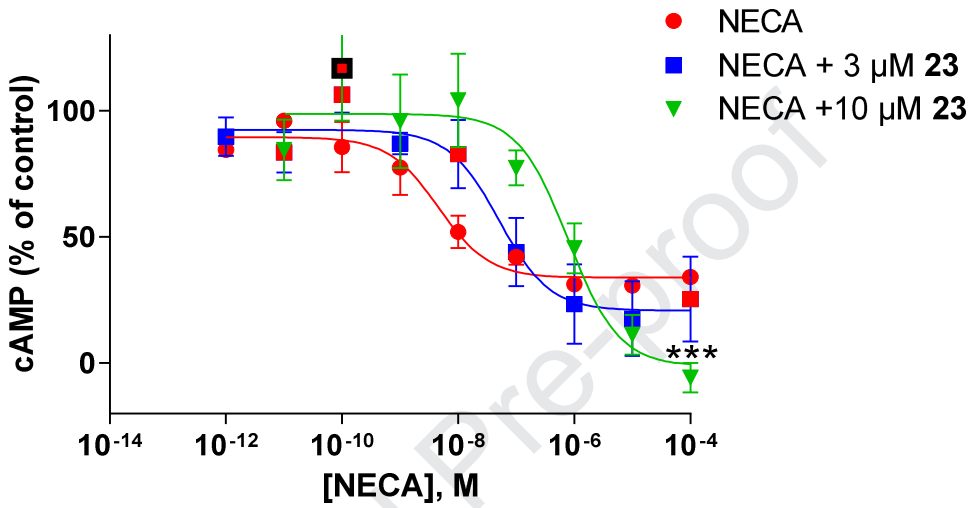

NECA effect	EC_{50} (nM)	% decrease in forskolin-stimulated cAMP accumulation
without inhibitor	**5.28** ± 3.43	66 ± 1
3 µM **23**	**56.9** ± 13.3	75 ± 17
10 µM **23**	**1720** ± 1070	95 ± 6

Fig. 6. Inhibition of forskolin (10 µM) induced cAMP production by NECA in CHO cells stably transfected with the rat A_3 AR, measured in the absence and presence of different concentrations (3 µM and 10 µM) of compound **23**. Data were normalized to forskolin (100%) and buffer (0%). NECA without inhibitor showed an EC_{50} value of 5.28 ± 3.43 with about 66% maximal inhibition of cAMP accumulation. NECA showed an EC_{50} values of 56.9 ± 13.3 and 1723 ± 1067 with maximal inhibition of cAMP accumulation of 75% and 95% upon addition of 3 µM and 10 µM of **23**. The calculated K_B value for compound **23** was 314 ±

92 nM (n=3). At the highest tested concentration of 10 µM of **23**, cAMP production was more strongly inhibited than by NECA alone possibly due to off-target effects.

GTP shift experiments

GTP shift experiments were performed for compounds **3**, **5**, **13** and **18** in order to determine whether they behave as agonists or antagonists at the A_1 AR. In general, GTP causes an uncoupling of the A_1 AR from the G_i protein leading to a shift of the receptor from the high- to the low-affinity state for agonists such as N^6-cyclopentyladenosine (CPA) [37]. In this experiment, the affinities of compounds were determined against the antagonist radioligand [^{3}H]DPCPX in the absence and in the presence of 100 µM GTP using rat brain cortical membrane preparations as previously described [37]. For the studied compounds **3**, **5**, **13** and **18** no significant shift of the binding curves in the absence or the presence of GTP was observed (Table 2). In contrast, the full agonist CPA showed a significant rightward shift of the binding curve of 8.3-fold in the presence of GTP (Fig. 7). Therefore, compounds **3**, **5**, **13** and **18** are clearly characterized as antagonists at A_1 ARs. Due to the structural similarity of all compounds in this series, we suppose that they all act as antagonists.

Table 2. Affinities and GTP shifts of selected compounds in comparison with the full agonist N^6-cyclopentyladenosine (CPA).

Compound	**IC_{50} ± SEM (nM)[a] (n = 3)**		
	-GTP	**+ 100 µM GTP**	**GTP shift[b]**
CPA	**64.7** ± 16.2	**537.6** ± 81.5	8.3 ± 3.6
3	**3.15** ± 2.48	**3.14** ± 2.59	0.9 ± 0.1
5	**0.0929** ± 0.019	**0.0981** ±0.036	1.0 ± 0.2
13	**0.0756** ± 0.009	**0.0763** ± 0.006	1.0 ± 0.1
18	**0.067** ± 0.024	**0.084** ± 0.028	1.3 ± 0.3

[a]Displacement of [^{3}H]DPCPX from rat cortical membranes.

[b]The affinities for the A_1 AR were determined in the absence and presence of 100 µM GTP. The GTP shifts were calculated by dividing the IC_{50} values determined in the presence of GTP by those measured in the absence of GTP.

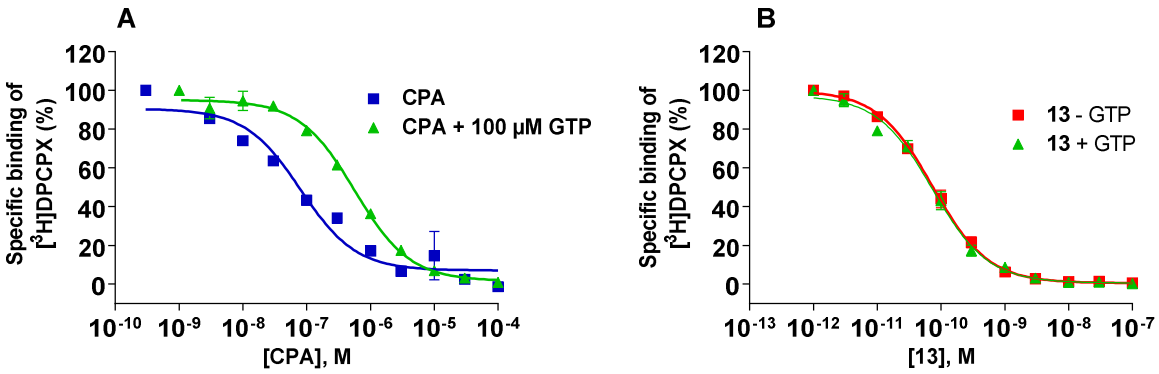

Fig. 7. Concentration–inhibition curves of the agonist CPA and compound **13** in the absence and presence of 100 µM GTP determined at rat A_1 ARs in brain cortical membrane preparations. [^{3}H]DPCPX (0.4 nM) was used as a radioligand.

The K_i value determined for compound **3** at the rat A_1 AR *vs.* the antagonist radioligand [^{3}H]DPCPX as compared to the agonist radioligand [^{3}H]CCPA was almost identical (2.93 nM and 2.79 nM, see Table 3). However, antagonists **5**, **13** and **18** showed about 10-fold higher affinity for A_1 ARs using the antagonist [^{3}H]DPCPX as a radioligand than vs. the agonist radioligand [^{3}H]CCPA (Table 3). DPCPX is an antagonist with inverse agonistic activity [52-54] which means that it prefers and stabilizes an inactive conformation of the A_1 AR, while agonists like CCPA show higher affinity for an activated receptor conformation and stabilize it. Our results indicate that the investigated A_1 AR antagonists **5**, **13**, and **18** behave as highly efficacious inverse agonists since their affinity for the [^{3}H]DPCPX-labeled receptor conformation is significantly higher than for the [^{3}H]CCPA-labeled, active conformation.

Table 3. Comparison of K_i values obtained for selected compounds at rat A_1ARs using the agonist radioligand [^{3}H]CCPA and the antagonist radioligand [^{3}H]DPCPX

Compounds	**K_i ± SEM (nM) at rat A_1 adenosine receptors**	
	[^{3}H]CCPA	**[^{3}H]DPCPX**
3	**2.79** ± 0.09	**2.93** ± 2.31
5	**0.939** ± 0.486	**0.0867** ± 0.0189
13	**0.529** ± 0.043	**0.0709** ± 0.094
18	**0.348** ± 0.134	**0.0628** ± 0.0228

Species differences

To analyze the observed species differences in more detail, the pK_i values of all potent compounds investigated in this study at human and rat A_1 or A_3 ARs, respectively, were correlated using a linear regression analysis (see Fig. 8). A high correlation (R^2 = 0.948; Fig. 8A) was observed for the human and rat A_1 AR, with consistently higher affinities for the rat species of about one order of magnitude. However, for the A_3 AR, for which less data were available, no correlation was observed, all compounds being less potent at the rat as compared to the human receptor (Fig. 8B).

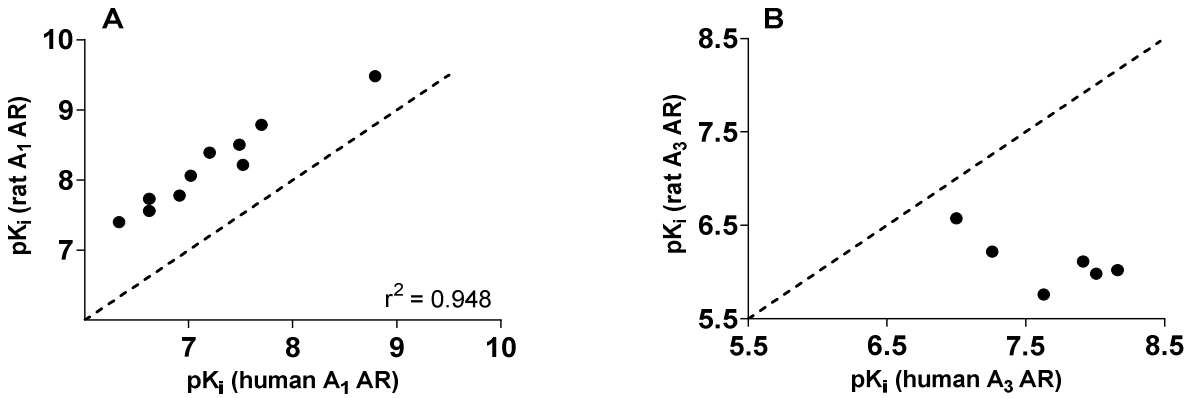

Fig. 8. Correlation of the pK_i values of rat versus human ARs. (A) correlation between human and rat A_1 ARs, (B) correlation between human and rat A_3 ARs.

In order to understand the observed species differences, amino acid sequences of the mouse, rat and human AR subtypes were aligned (see Table S1 of Supporting Information (SI)). Sequence differences between AR subtypes are ranging from 39-61% (human) and a very similar range is observed for rat and mouse (see Table S1, left column). A_{2A} and A_{2B} ARs are the most closely related subtypes (>60% sequence identity in human, rat and mouse). A_{2A}/A_{2B} compared to A_3 ARs are the most dissimilar subtypes with only 38-40% sequence identity. Although the amino acid sequences of A_1, A_{2A} and A_{2B} ARs are highly conserved between rat, mouse and human (e.g. human, rat and mouse A_1 ARs are 95% identical, Table S1, right column), the A_3 ARs of rodents (rat, mouse) and humans share only 72% identity, which determines the observed differences in ligand affinities.

Molecular modeling studies

In order to rationalize the potency and selectivity profile obtained for the 2-amino-4-phenylthiazole derivatives, we performed molecular docking and molecular dynamics simulation studies using the crystal structure of the human A_1 AR (PDB ID: 5N2S) and a homology model of the human A_3 AR [29]. We selected the two potent antagonists **17** (A_3-selective), and **18** (dual A_1/A_3 antagonist) (see Table 1).

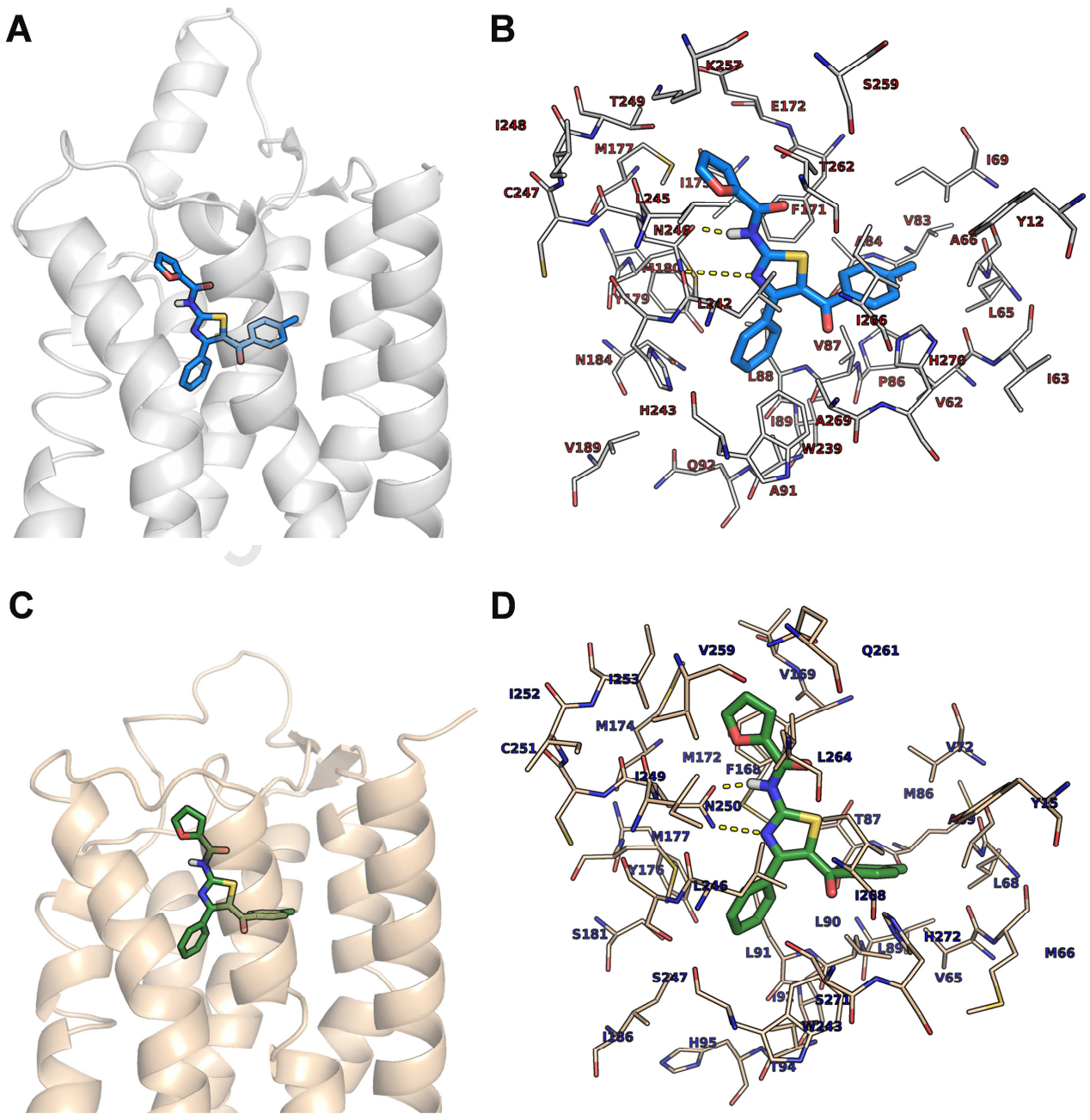

Fig. 9. Putative binding modes of the dual A_1/A_3 antagonist **18** in the crystal structure of the human A_1 AR (**A**, **B**) and in the homology model of the human A_3AR (**C**, **D**) depicting residues that may be important for the interaction. The human A_1AR and the human A_3 AR are displayed in cartoon representation. Carbon atoms of **18** are colored cyan and green, the important residues are colored in gray and pink, respectively. Oxygen atoms are colored in red, nitrogen atoms in blue, and sulfur atoms in yellow.

Compound **18**, a 2-amino-4-phenylthiazole derivative containing a furyl group as R^1 and a 4-methylbenzoyl group at position R^2 shows high potency towards both the human A_1 AR and the human A_3 AR. The selected compound was docked into the orthosteric binding site of both receptors using Autodock 4.2. The putative binding mode of **18** and important residues in the binding site of the human A_1 AR are shown in Fig. 9A and B. The compound was anchored inside the binding site by two strong hydrogen bonding interactions between N3 of the thiazole ring and NH of the carboxamido group of **18** with the amide moiety of Asn246. The thiazole ring is predicted to additionally form a strong hydrophobic π-π interaction with Phe171. Upon further analysis of the binding pose of **18**, the compound was predicted to occupy three subpockets (A-C, see Fig. S2 in Supporting Information). The phenyl group at position 4 of the thiazole ring occupies subpocket A formed by the hydrophobic residues V87, L88, A91, F171, M180, W247 and L250 and by two polar residues H251 and N254, which stabilize compound **18** in the model through hydrophobic interactions. The respective binding subpocket in the human A_{2A} AR is narrower and cannot accommodate a phenyl ring [29]. This is supported by the biological investigations which showed low potency of **18** at the A_{2A}AR (Table 1). The amino acid residues in the human A_{2B} AR are similar to that in the A_{2A} AR, and this is a likely explanation why **18** was found to be also inactive at the A_{2B} AR.

The 4-methylbenzoyl group (R^2) is proposed to be positioned in subpocket B of the human A_1 AR, which is limited in size, interacting with another set of residues including V62, L65, A66,

V83, A84, V87, F171, L250 and H278. Large substituents, e.g. quinazolin-4-one derivatives included in a number of compounds (**6-9, 15-17, 20-23**), cannot be accommodated in subpocket B of the human A_1 AR (see Table 1 for structures and binding affinity values). However the potency values of the compounds with large substituents is also depending on the substitution at R^1 which occupies subpocket C, because the smaller substitutions at R^2 might induce alternative binding poses and introduce steric clashes at subpocket C. Subpocket C located below extracellular loop (ECL) 3 is occupied by the 2-furyl group substituted at R^1 of **18**. Subpocket C is formed by a mixture of hydrophobic and polar residues which include Phe171, Glu172, Met177, Leu250, Leu253, Thr257, Lys265 and Thr270. Specifically, the amino acid residues in ECL3 are unique for each of the AR subtypes and in each species. The residues of ECL3 contribute largely to subtype and species selectivity, and particularly large differences are found between the ECL3 of the human and the rat A_3 AR.

As shown in Fig. 9C and D, compound **18** follows a similar interaction pattern for the thiazole ring in the human A_3 AR as in the A_1 AR. It forms hydrogen bond and hydrophobic interactions with Asn250 and Phe168, respectively, and the substitutions at position 4 (phenyl), R^2 (*p*-methylbenzoyl group) and R^2 (2-furyl group) of **18** were observed to occupy the three subpockets A, B and C, respectively, in the model. These interactions are assumed to stabilize **18** in the binding site of the human A_3 AR with slight variations in the amino acid residues in comparison to the human A_1 AR. (See Fig. S1 for sequence alignment). Although similar amino acids exist in the subpockets A and B of both receptor subtypes, subpocket C located below the ECL3 of the human A_3AR differs largely in comparison to the human A_1 AR. Furthermore, the polar residues Thr257 and Thr270 (human A_1 AR) are replaced by Ile253 and Leu264 (human A_3 AR) which alters the polarity of the subpocket. This could contribute to the approximately 6-fold decrease in binding affinity of **18** at the human A_3 AR (K_i 42.2 nM) in comparison to the human A_1 AR (K_i 7.57 nM). Thus in addition to key

hydrogen bond and hydrophobic interactions, the substitution which provides a tighter binding in subpocket B is important for the potency, and substitution at the part binding in subpocket C and interaction of amino acid residues from ECL3 are likely responsible for selectivity.

As a next step, we performed molecular dynamics simulations of the two complexes for explaining the stabilities of the predicted binding poses of **18** in the binding sites of the human A_1 AR and the A_3 AR (see Supplementary Video S1 and S2). For both complexes, the calculated root mean square deviation (RMSD) values of the Cα atoms of the complexes rapidly reached an equilibrium state with approximately 1 Å deviation from the first frame of 100 ns simulations. The visual analysis of the trajectories obtained for the two complexes shows that compound **18** was anchored inside the binding site with the interaction pattern identified from the docking studies (Fig. S3 and Fig. S4). It maintains the key hydrogen bond interaction with an asparagine residue (Asn246 and Asn250 in the human A_1 AR and the A_3 AR, respectively), and hydrophobic interactions with a phenylalanine residue (Phe171 and Phe168). The root mean square fluctuation (RMSF) values of the two receptors, the human A_1 AR and A_3 AR, showed a profile with large fluctuations only appearing in the loop regions indicating a similar mechanism of interaction of the ligand with both receptors. Furthermore, an ionic lock is predicted to be formed in the human A_1 AR between Glu172 from ECL2 and Lys265 of ECL3 acting as a cap for subpocket C to which compound **18** binds, helping the compound to bind tightly inside the binding pocket. Similarly, an ionic lock was previously detected in the human A_{2A} AR formed between Glu169 and His264, which contributed to variations in dissociation kinetics [54]. On the contrary, the amino acids Glu172 and Lys265 of the human A_1 AR are replaced by Gln167 and Val259 in the human A_3 AR resulting in a loss of ionic lock formation and formation of a binding cap in subpocket C. Due to the absence of an ionic lock and loose, flexible binding of the *p*-methylbenzoyl group, the key

hydrogen and hydrophobic interactions with Asn250 and Phe168 may be weakened in the A_3 AR.

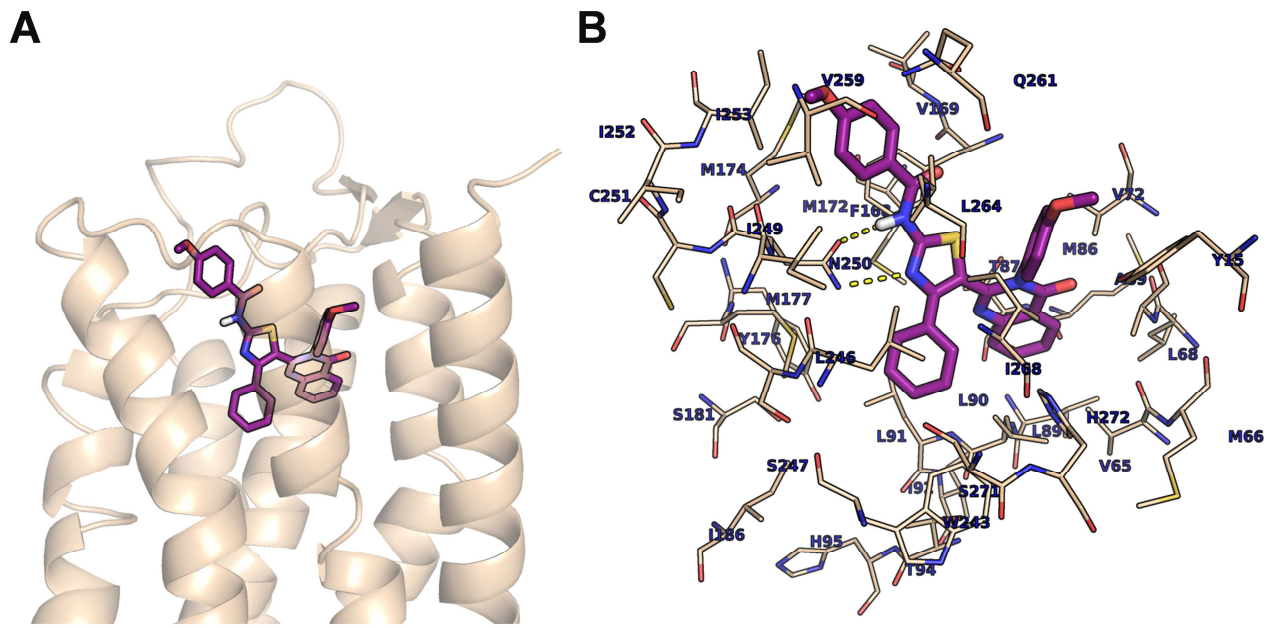

Fig. 10. **A**. Putative binding modes of **17** in the homology model of the human A_3 AR. **B**. Residues predicted to be important for the binding interaction are shown. The human A_3 AR is displayed by cartoon representation. Carbon atoms of **17** are colored in magenta and the important residues for binding to the A_3 AR are colored in pink. For color coding of other atoms see Fig. 9.

The second selected antagonist, **17**, with a 4-methoxyphenyl residue as R^1 and a 3-(4-methoxyphenyl)quinazolin-4-one residue as R^2 shows high potency and selectivity for the human A_3 AR (see Table 1). The docked pose of **17** and important residues in the binding pocket of the human A_3 AR model are shown in Fig. 10A and B. Similar to compound **18**, hydrogen bond interactions with Asn250 and a possible hydrophobic interaction with Phe168 are conceivable. Compound **17** is predicted to also occupy the three subpockets A, B and C in the binding site. Due to larger substitution at position R^2 in **17**, subpocket B is almost

completely occupied in comparison to **18**. In addition to the substitution at position 3 of quinazolin-4-one derivatives, the potency for the human A_3 AR depends on the substitutent R^1.

Similar to compound **18**, we performed molecular dynamics simulations of the human A_3 AR in complex with compound **17** to investigate the stability of the predicted binding pose of **17** in the binding site of the human A_3 AR (see Supplementary Video S3). The RMSD and RMSF values showed a similar profile as observed before for compound **18** (Fig. S3 and Fig. S4). The amino acid residues of the receptor reached the equilibrium state with approximately 1 Å deviation from the first frame of 100 ns simulations, and large fluctuations only appeared in the loop regions.

Conclusions

In conclusion, we synthesized and optimized a series of novel 4-phenylthiazole derivatives with the aim to enhance A_1 and/or A_3 AR affinity and selectivity versus the other AR subtypes. Highly potent and subtype-selective A_1 AR antagonists (e.g. **13**) as well as A_3 AR antagonists (e.g. **17**, **23**) were obtained. In addition, we were successful in developing dual A_1/A_3 AR antagonists (**10**, **18**). Species differences (human – rat) were studied, and A_1 AR affinity was found to be generally higher at the rat than at the human orthologue, while the opposite was observed for the A_3 AR subtype. Functional properties of selected compounds were evaluated which indicated that the the compounds behaved as antagonists at A_1 and A_3 AR with inverse agonistic activity, which was proven for the A_1 AR. Docking and molecular dynamics studies served to explain the observed SARs, species differences and receptor subtype selectivities.

Experimental section

General information

All commercially available reagents were obtained from various producers (Sigma-Aldrich, SD Fine, Spectrochem, Merck and Himedia) and used without further purification. The reactions were monitored and the purity of the compounds was checked by thin layer chromatography (TLC) using aluminum sheets with silica gel 60 F_{254} (Merck). Mass spectra were recorded on an API 2000 (Applied Biosystems, Darmstadt, Germany) mass spectrometer (turbo ion spray ion source) coupled with an HPLC system (Agilent 1100) using a Phenomenex Luna 3µ C18 column. ^{1}H- and ^{13}C-NMR were recorded at the University of Pittsburgh, USA on a Bruker Avance 600 MHz instrument. DMSO-d_6, $CDCl_3$ or MeOD were used as solvents as indicated below. Chemical shifts are given in ppm relative to the remaining protons of the deuterated solvents used as internal standard. Melting points were determined on VEEGO-VMP I melting point apparatus and are uncorrected. Infrared spectra were recorded on JASCO-FTIR 4100 spectrophotometer. The purity of the compounds was checked by dissolving 1 mg/mL in MeOH containing 2 mM ammonium acetate. A sample of 10 µL was injected into an HPLC instrument (Agilent 1100) using a Phenomenex Luna 3µ C18 column. Elution was performed with a gradient of water : methanol (containing 2 mM ammonium acetate) from 60 : 0 to 40 : 100 for 30 min followed by 10 min of 100% MeOH at a flow rate of 250 µL/min. UV absorption for each compound was detected at 254 nm. The purity of the products was generally ≥ 95.

(*E*)-*N*-((Diethylamino)(phenyl)methylenecarbamothioyl)benzamide (**2b**) and (*E*)-*N*-((diethylamino)(phenyl)methylenecarbamothioyl)furan-2-carboxamide (**2c**) were synthesized as previously described (for details see SI) [41].

General procedure for the preparation of amidinothiourea derivatives 2a-c

To a stirred solution of isothiocyanate (1 equivalent) in acetone and to it an amidine (1 equivalent) was added dropwise while keeping the temperature between 0–5 °C. After completion of amidine addition, the reaction mixture was warmed to 15–20 °C until the products precipitated. Products were washed with cold acetone and dried under vacuum to give **2a-c** in 65-80% yield.

General procedure for the preparation of thiazole derivatives 3-23

To a solution of 1 mmol of the amidinothiourea derivatives **2a-c** in 2 mL of acetonitrile (for compounds **4** and **9** methanol was used as solvent) was added 1 mmol of 2-bromo-1-(aryl)ethanone derivatives or 2-(chloromethyl)-3-(aryl)quinazolin-4(3*H*)-one derivatives and the reaction mixture was stirred at rt for 1 h. Pure products precipitated and were filtered off and dried.

(*E*)-*N*-((Diethylamino)(phenyl)methylenecarbamothioyl)-4-methoxybenzamide (2a). IR (KBr cm^{-1}); 3350, 3145.35, 2973.7, 1681.62, 1500, 1480; m.p. 128-130 °C. Yield 78%.

***N*-(5-(2,4-Difluorobenzoyl)-4-phenylthiazol-2-yl)benzamide (3).** ^{1}H-NMR (600 MHz, DMSO-d_6) δ 6.99 (d, 2H), 7.1 (m, 3H), 7.2 (s, 1H), 7.3 (s, 1H), 7.5 (t, 3H), 7.6 (s, 1H), 8.1 (d, 2H), 13.34 (s, 1H). ^{13}C-NMR (150 MHz, DMSO-d_6) δ 104.34, 112.05, 124.42, 127.03, 128.03, 129.20, 130.01, 131.77, 132.77, 133.65, 134.07, 157.20, 159.0, 160.80, 162.30, 163.47, 166.88, 184.75. IR (KBr cm^{-1}); 3270.68, 3041.19, 1686.44, 1614.13, 1580, 1500, 1480, 1350. HRMS (ESI, $[M+Na]^+$); Found: 443.0661, Calcd.: 443.0642. LC/ESI-MS negative mode 419.4 ($[M-H]^-$), positive mode 421.4 ($[M+H]^+$). LC/ESI-MS purity 98.8%. m.p. 230-232 °C. Yield 67%.

***N*-(4-Phenyl-5-(pyridin-2-yl)thiazol-2-yl)benzamide (4).** ^{1}H-NMR (600 MHz, MeOD) δ 7.4-7.5 (m, 5H), 7.5 (t, 3H), 7.6-7.8 (m, 3H), 8.0 (d, 2H), 8.6 (s, 1H), 13.14 (s, 1H). IR (KBr cm^{-1}); 3093.26, 2890.23, 2000, 1659.22, 1645.23, 1600, 1540, 1480. HRMS (ESI, [M+1]); Found: 358.1029, Calcd.: 358.1014. LC/ESI-MS negative mode 356.4 ($[M-H]^-$), positive mode 358.3 ($[M+H]^+$). LC/ESI-MS purity 98.7%. m.p. 224-226 °C. Yield 38%.

***N*-(5-(4-Chlorobenzoyl)-4-phenylthiazol-2-yl)-4-methoxybenzamide (11).** ^{1}H-NMR (600 MHz, DMSO-d_6) δ 3.85 (s, 3H), 7.09 (d, 2H), 7.21 (m, 5H), 7.26 (d, 2H), 7.29 (d, 2H), 8.16 (d, 2H), 13.10 (s, 1H). ^{13}C-NMR (150 MHz, DMSO-d_6) δ 56, 114, 123, 125, 128.3, 128.5, 129.1, 130, 131, 131.3, 134, 136, 137, 155, 161, 163, 165, 188.1. IR (KBr cm^{-1}); 3317.93, 3056.62, 2950, 1660.41, 1625, 1590, 1479. HRMS (ESI, [M+Na]); Found: 471.0559, Calcd.: 471.0570. LC/ESI-MS negative mode 447.2 ($[M-H]^-$), positive mode 449.3 ($[M+H]^+$). LC/ESI-MS purity 96.9%. m.p. 260-262 °C. Yield 96%.

4-Methoxy-*N*-(5-(4-methoxybenzoyl)4-phenylthiazol-2-yl)benzamide (12). ^{1}H-NMR (600 MHz, DMSO-d_6) δ 3.75 (s, 3H), 3.85 (s, 3H), 6.83 (d, 2H), 7.0 (d, 2H), 7.2 (m, 3H), 7.4 (d, 2H), 7.6 (d, 2H), 8.1 (d, 2H), 13.0 (s, 1H). ^{13}C-NMR (150 MHz, DMSO-d_6) δ 55.96, 113.0, 114.0, 128.3, 128.7, 129.7, 130.8, 131.0, 132.2, 135.0, 163.0, 188.0. IR (KBr cm^{-1}); 3285.14, 3062.36, 2600.33, 1603.63, 1580, 1500, 1490. HRMS (ESI, [M+Na]); Found: 467.1032, Calcd.: 467.1041. LC/ESI-MS negative mode 443.4 ($[M-H]^-$), positive mode 445.3 ($[M+H]^+$). LC/ESI-MS purity 95%. m.p. 226-228 °C. Yield 63%.

4-Methoxy-*N*-(5-(4-methylbenzoyl)-4-phenylthiazol-2-yl)benzamide (13). ^{1}H-NMR (600 MHz, DMSO-d_6) δ 2.27 (s, 3H), 3.86 (s, 3H), 7.1 (m, 4H), 7.2 (m, 3H), 7.4 (d, 2H), 7.5 (d, 2H), 8.1 (d, 2H), 13.0 (s, 1H). ^{13}C-NMR (150 MHz, DMSO-d_6) δ 56.05, 114.4, 123.8, 125, 128.3, 129, 129.2, 129.8, 130.9, 134.7, 135.5, 143.4, 154.3, 160.8, 163.5, 165.5, 189.2. IR

(KBr cm^{-1}); 3317.93, 3051.80, 2990, 1660.41, 1590.2, 1500, 1479. LC/ESI-MS negative mode 427.4 ($[M-H]^-$), positive mode 429.3 ($[M+H]^+$). LC/ESI-MS purity 96.6%. m.p. 224-226 °C. Yield 55%.

***N*-(5-(2,4-Difluorobenzoyl)-4-phenylthiazol-2-yl)-4-methoxybenzamide (14).** ^{1}H-NMR (600 MHz, $CDCl_3$) δ 3.91 (s, 3H), 6.45 (s, 1H), 6.7 (s, 1H), 7.0 (d, 2H), 7.1 (d, 2H), 7.2 (m, 3H), 7.3 (s, 1H), 7.4 (d, 2H), 9.68 (s, 1H). ^{13}C-NMR (150 MHz, $CDCl_3$) δ 55.56, 114.4, 127.7, 129.5. IR (KBr cm^{-1}); 3327.57, 3073.01, 2850.30, 1660.41, 1600.25, 1550, 1500, 1480. HRMS (ESI, [M+Na]); Found: 473.0793, Calcd.: 473.0747. LC/ESI-MS negative mode 449.2 ($[M-H]^-$), positive mode 451.5 ($[M+H]^+$). LC/ESI-MS purity 99.0%. m.p. 240-242 °C. Yield 78%.

4-Methoxy-*N*-(5-(4-oxo-3-phenyl-3,4-dihydroquinazolin-2-yl)-4-phenylthiazol-2-yl)benzamide (15). ^{1}H-NMR (600 MHz, $CDCl_3$) δ 3.8 (s, 3H), 6.6 (d, 2H), 6.9 (d, 2H), 7.0 (d, 2H), 7.1 (d, 1H), 7.18 (m, 3H), 7.25 (t, 1H), 7.26 (t, 1H), 7.3 (d, 1H), 7.5 (m, 3H), 8.35 (d, 2H), 9.69 (s, 1H). ^{13}C-NMR (150 MHz, $CDCl_3$) δ 55.56, 114.2, 119.7, 121.3, 123.5, 127.3, 127.8, 127.9, 128.2, 128.4, 128.5, 128.8, 129.5, 133.9, 134.9, 136.2, 147.2, 148.4, 148.7, 158.4, 162.1, 163.4, 164.2. IR (KBr cm^{-1}); 3250.90, 3062.41, 2843.52, 1675.36, 1600, 1550, 1500, 1480. HRMS (ESI, [M]); Found: 530.14, Calcd.: 530.14. LC/ESI-MS negative mode 529.4 ($[M-H]^-$), positive mode 531.7 ($[M+H]^+$). LC/ESI-MS purity 96.3%. m.p. 268-270 °C. Yield 74%.

4-Methoxy-*N*-(5-(4-oxo-3-p-tolyl-3,4-dihydroquinazolin-2-yl)-4-phenylthiazol-2-yl)benzamide (16). ^{1}H-NMR (600 MHz, $CDCl_3$) δ 2.24 (s, 3H), 3.87 (s, 3H), 6.50 (d, 2H), 6.8 (m, 4H), 6.9 (t, 3H), 7.2 (d, 2H), 7.5-7.8 (m, 4H), 8.3 (d, 2H), 9.92 (s, 1H). ^{13}C-NMR (150 MHz, $CDCl_3$) δ 55.55, 114.2, 118.4, 119.9, 121.3, 123.3, 127.3, 127.5, 127.7, 127.8, 127.9,

128.5, 128.7, 129.1, 129.4, 133.6, 134, 138.2, 147, 148.6, 162.3, 163.5. IR (KBr cm^{-1}); 3250, 3067.23, 2837.74, 1692.23, 1620, 1556, 1489. HRMS (ESI, [M+Na]); Found: 567.1509, Calcd.: 567.1467. LC/ESI-MS negative mode 543.4 ($[M-H]^-$), positive mode 545.5 ($[M+H]^+$). LC/ESI-MS purity 98.7%. m.p. 274-276 °C. Yield 42%.

4-Methoxy-*N*-(5-(3-(4-methoxyphenyl)-4-oxo-3,4-dihydroquinazolin-2-yl)-4-phenylthiazol-2-yl)benzamide (17). ^{1}H-NMR (600 MHz, $CDCl_3$) δ 3.72 (s, 3H), 3.89 (s, 3H), 6.5 (d, 4H), 6.9 (d, 2H), 7.2 (m, 5H), 7.3-7.8 (m, 4H) 8.3 (d, 2H), 9.60 (s, 1H). ^{13}C-NMR (150 MHz, $CDCl_3$) δ 55.58, 113.7, 114.3, 119.9, 121.3, 123.3, 127.3, 127.7, 127.8, 128, 128.6, 128.8, 128.9, 129, 129.4, 134.1, 134.8, 136.7, 147.2, 148.6, 148.8, 157.9, 159, 162.4, 163.5, 163.8. IR (KBr cm^{-1}); 3310, 3062.41, 2843.52, 1697.05, 1600, 1569, 1510, 1458. HRMS (ESI, [M+Na]); Found: 583.1413, Calcd.: 583.1416. LC/ESI-MS negative mode 559.4 ($[M-H]^-$), positive mode 561.5 ($[M+H]^+$). LC/ESI-MS purity 97.6%. m.p. 262-264 °C. Yield 88%.

***N*-(5-(4-Methylbenzoyl)-4-phenylthiazol-2-yl)furan-2-carboxamide (18).** ^{1}H-NMR (600 MHz, DMSO-d_6) δ 2.39 (s, 3H), 6.6 (d, 2H), 7.0 (t, 3H), 7.1 (d, 2H), 7.2 (d, 2H), 7.5 (m, 3H), 9.7 (s, 1H). ^{13}C-NMR (150 MHz, DMSO-d_6) δ 115, 118, 124, 125, 128, 135, 139, 142, 146, 148, 150, 158, 190, 210. IR (KBr cm^{-1}); 3235, 3125.23, 16 69.45, 1600, 1590.36, 1550, 1467. HRMS (ESI, [M+Na]); Found: 411.0783, Calcd.: 411.0779. LC/ESI-MS negative mode 387.4 ($[M-H]^-$), positive mode 389.4 ($[M+H]^+$). LC/ESI-MS purity 97.3%. m.p. 200-202 °C. Yield 36%.

***N*-(5-(2,4-Difluorobenzoyl)-4-phenylthiazol-2-yl)furan-2-carboxamide (19).** ^{1}H-NMR (600 MHz, $CDCl_3$) δ 6.4 (d, 1H), 6.45 (d, 1H), 6.6 (d, 1H), 7.1 (d, 2H), 7.2-7.4 (m, 3H), 7.5 (m, 3H), 9.7 (s, 1H). ^{13}C-NMR (150 MHz, $CDCl_3$) δ 106, 108, 110, 118, 122, 124, 126, 130,

132, 138, 142, 144, 156, 158, 160, 182, 220. IR (KBr cm^{-1}); 3255.25, 3100.36, 1676.81, 1600, 1530.24, 1500, 1489. HRMS (ESI, [M+Na]); Found: 433.0435, Calcd.: 433.0434. LC/ESI-MS negative mode 409.3 ($[M-H]^-$), positive mode 411.3 ($[M+H]^+$). LC/ESI-MS purity 98.0%. m.p. 190-192°C. Yield 42%.

Radioligand binding assays

Assays were performed as previously described [46, 47, 50, 55, 56]. Membrane preparations of CHO cells expressing human A_1, human A_{2A}, human or rat A_{2B} and human or rat A_3 ARs were used as described before [47, 48, 51]. For some experiments, commercially available membrane preparations of HEK293 cells expressing the human A_{2A} AR obtained from PerkinElmer (Product No.: RBHA2AM400UA) were employed. Rat brain cortical membrane preparations were used for rat A_1 AR, and rat brain striatal membrane preparations for rat A_{2A} AR binding assays; membrane preparations were obtained as previously described [56, 57]. Competition binding experiments was performed using [^{3}H]2-chloro-N^6-cyclopentyladenosine ([^{3}H]CCPA (58 Ci/mmol), 0.5 nM (rat and human A_1 AR) [48], [^{3}H]3-(3-hydroxypropyl)-7-methyl-8-(*m*-methoxystyryl)-1-propargylxanthine ([^{3}H]MSX-2 (84 Ci/mmol), 1.0 nM (rat and human A_{2A} AR) [49], [^{3}H]8-(4-(4-(4-chlorophenyl)piperazine-1-sulfonyl)phenyl)-1-propylxanthine [^{3}H]PSB-603 (73 Ci/mmol), 0.3 nM (rat and human A_{2B} AR) [45], [^{3}H]phenyl-8-ethyl-4-methyl-(8*R*)-4,5,7,8-tetrahydro-1*H*-imidazo[2,1-i]purine-5-one ([^{3}H]PSB-11 (53 Ci/mmol), 0.5 nM (human A_3 AR) [48], and [^{3}H]1-(6-amino-9*H*-purin-9-yl)-1-deoxy-*N*-ethyI-*β*-D-ribofuronamide) ([^{3}H]NECA, 15.5 Ci/mmol), 10 nM (rat A_3 AR). Nonspecific binding was determined using 10 µM of 2-chloroadenosine (CADO) for A_1 AR assays, 50 µM of 5'-(*N*-ethylcarboxamido)adenosine (NECA) for A_{2A} AR assays, and 100 µM of (*R*)-N^6-phenyl-isopropyladenosine (*R*-PIA) for A_3 AR assays. The binding assays (except for A_{2B} AR assays) were performed in a total volume of 400 µl of assay buffer (50 mM TRIS-HCl, pH 7.4). Stock solutions of test compounds were prepared in dimethyl sulfoxide

(DMSO); the final DMSO concentration was 2.5%. The A_{2B} AR binding assays were carried out in 1000 µl total volume of assay buffer, and nonspecific binding was determined in the presence of 10 µM 8-cyclopentyl-1,3-dipropylxanthine (DPCPX). The membrane preparations were preincubated for 20 min with adenosine desaminase (ADA) 2 U/mL per mg of protein. Incubation was carried out at rt for 90 min (A_1 AR assays), for 30 min (A_{2A} AR assays), for 75 min (A_{2B} AR assays), or for 60 min (A_3 AR assays), respectively. The incubation was terminated by rapid filtration through GF/B glass fiber filters using a 48-channel cell harvester (Brandel), and filters were washed three times with ice-cold TRIS-HCl buffer (50 mM, pH 7.4), which contained 0.1% bovine serum albumin (BSA) in case of the A_{2B} AR binding assays. The filters were transferred into scintillation vials and incubated for 6 h with 2.5 mL of scintillation cocktail (Beckman Coulter). Radioactivity was counted in a liquid scintillation counter. At least three separate experiments were performed, each in duplicate or triplicate.

GTP shift assay

[^{3}H]8-cyclopentyl-1,3-dipropylxanthine ([^{3}H]DPCPX, 120 Ci/mmol, 0.4 nM) was used as a radioligand in GTP shift assays at rat A_1 ARs, and the GTP shift was measured in the presence of 100 µM GTP. Nonspecific binding was determined using 10 µM of DPCPX. The assays were carried out under the same conditions as described above for the A_1 AR competition assay as previously described [37].

cAMP accumulation assay

Cells stably expressing the A_3 AR were cultured in 24-well plates (150,000-200,000 cell/well). After removal of the culture medium, cells were washed with HBSS (containing 20 mM HEPES buffer, pH 7.3) and then incubated with the same buffer, containing 2U/ml

adenosine deaminase for 2 h at 37 °C. Forskolin (10 µM) and different concentrations of the agonist NECA were added to the cells at 36.5 °C. After incubation, the reaction was stopped by removal of the reaction buffer followed by the addition of a hot lysis solution (500 µl, 90 °C, Na_2EDTA (4 mM), Triton X100 (0.1 ‰)). Then, the assay was completed as described before [58, 59].

Data analysis

Data were analyzed using GRAPHPAD PRISM Version 4 (San Diego, CA, USA). For the calculation of K_i values by nonlinear regression analysis, the Cheng-Prusoff equation and K_D values for [^{3}H]CCPA of 0.2 nM (rat A_1 AR), 0.61 nM (human A_1 AR), and for [^{3}H]MSX-2 of 8 nM (ratA_{2A} AR) and 7.3 nM (human A_{2A} AR), and for [^{3}H]PSB-603 of 0.41 nM (human A_{2B} AR), 0.2 nM (rat A_{2B} AR), and for [^{3}H]PSB-11 of 4.9 nM (human A_3 AR) were used.

Homology Modelling

The X-ray crystal structure of human A_1 adenosine receptor (hA_1 AR) with the antagonist PSB-36 (PDB ID: 5N2S.pdb) was downloaded from RSCB Protein Data Bank (http://www.rcsb.org/) [60]. The structure was used as a template for generating a homology model of the human A_3 AR using Modeller9 [61]. The amino acid sequence of the human A_3 AR with the accession number P0DMS8 was retrieved from UniProt sequence database (http:// http://www.uniprot.org/). The overall sequence similarity of 68.1% and identity of 47.7% between the human A_1 AR and the human A_3 AR was reasonable and justified the choice of the human A_1 AR structure as a template for the homology model of the human A_3 AR. The sequences were aligned using the alignment tool ClustalOmega [62]. The alignment was visually interpreted for further improvement. The resulting alignment was used as input to the Modeller9 program and optimized using the variable target function method (VTFM)

[61]. From the 100 generated models, the Discrete Optimized Protein Energy (DOPE) score was utilized to select the best model for the human A_3 AR [61, 63]. The protonation of the selected models was done using the Protonate3D algorithm using the Molecular Operating Environment (MOE 2018.01) followed by minimization with a root mean square of 0.5 Å [64]. The overall structural quality was confirmed by a Ramachandran Plot, and sequence-structure compatibility of the model was ensured using PROSA II profile analysis [65, 66].

Molecular docking

The crystal structure of the human A_1 AR and the homology model of human A_3 AR were applied for flexible ligand docking using AutoDock 4.2 [67]. During the docking simulations, the ligands were fully flexible and the residues of the receptor were treated as rigid. Selected compounds were docked into the active site of human A_1 AR and A_3 AR to predict the binding modes of the compounds. The atomic partial charges were added using AutoDockTools [67, 68]. Fifty independent docking calculations using the *var*CPSO-ls algorithm from PSO@Autodock implemented in AutoDock4.2 were performed and terminated after 500,000 evaluation steps [69]. Parameters of *var*CPSO-ls algorithm, the cognitive and social parameters were set to 6.05 with 60 individual particles as swarm size. All the other parameters of the algorithm were set to their default values. Possible binding modes of the compounds were explored by visual inspection of the resulting docking poses.

Molecular dynamic simulations

The receptor-ligand complexes for molecular dynamics (MD) simulations was prepared using the Bilayer builder of the Membrane builder module implemented in CHARMM–GUI [70-71]. The docked complexes were solvated with transferable intermolecular potential 3P (TIP3P) water molecules [72] and neutralized by adding Na^+/Cl^- counter-ions to a final concentration of 0.15 M. The MD simulation was carried out using the CHARMM36 /

CGenFF (3.0.1) force fields for protein and ligand atoms, respectively, and periodic boundaries [73-74]. Ligand parameters were generated using the ParamChem service (https://cgenff.paramchem.org) implemented in CHARMM-GUI. The complexes were subjected to equilibration procedure using NAMD [75] over a period of 5 ns using the input files generated from CHARMM-GUI. During the simulations, non-bonded interactions were gradually switched off at 10 Å, and the long-range electrostatic interactions were calculated using the Particle-mesh Ewald method [76]. The temperature was maintained at 303.15 K using the Langevin thermostat, and the pressure was maintained at 1 atm using a Berendsen barostat. Bond lengths involving hydrogen atoms were constrained using the M-SHAKE algorithm. The equilibrated systems were subjected to 100 ns of unrestrained MD simulations run in triplicate for MRGPRX2-RMC40 complex with the ACEMD engine (Acellera, High Throughput Molecular Dynamics) [77] For every 0.4 ns a frame was written into the trajectory file. MD trajectory analysis was performed with an in-house script exploiting the RMSD trajectory tool implemented in VMD (Version 1.9.3) [78]. The Cα atoms of the human A_1 and A_3 AR were taken into account in the RMSD plot and for visualizing the fluctuation in the RMSF plot.

Acknowledgements

We acknowledge the contributions by Kamala K Vasu, V. Sudarsanam and Gajanan Inamdar of B.V. Patel PERD Center, Ahmedabad, in the design and synthesis of the compounds **11**, **12**, and **13** studied in this work. Marion Schneider is gratefully acknowledged for recording mass spectra. This manuscript was supported by the European Commission within the COST Action MuTaLig (CA15135).

Supplementary material available:

Synthetic schemes, experimental procedures, ^{1}H-, ^{13}C-NMR, IR and MS spectral data for compounds **2b-c**, **5-10** and **20-23**, for reagents and intermediate products. HPLC(ESI)MS purity data for selected thiazoles. Sequence comparison of different AR subtypes and different species; comparison of putative binding poses of selected compounds in the human A_1 and A_3 AR, respectively; molecular dynamics simulations of A_1 and A_3 AR complexes with selected antagonists.

References

[1] B. B. Fredholm, A. P. IJzerman, K. A. Jacobson, J. Linden, C. E. Müller. International Union of Basic and Clinical Pharmacology. LXXXI. Nomenclature and classification of adenosine receptors-an update. Pharmacol. Rev. 63 (2011) 1–34.

[2] C. E. Müller, K. A. Jacobson. Recent developments in adenosine receptor ligands and their potential as novel drugs. Biochim. biophys. acta 1808 (2011) 1290–1308.

[3] K.A.Jacobson, D. K. Tosh, S. Jain, Z. G. Gao. Historical and current adenosine receptor agonists in preclinical and clinical development. Front Cell Neurosci. 28 (2019) 13-124.

[4] L. V. Lopes, A. M. Sebastiao, J. A. Ribeiro. Adenosine and related drugs in brain diseases: present and future in clinical trials. Curr. Top. Med. Chem. 11 (2011) 1087–1101.

[5] G. Burnstock, U. Krügel, M. P. Abbracchio, P. Illes. Purinergic signalling: from normal behaviour to pathological brain function. Prog. Neurobiol. 95 (2011) 229–274.

[6] K. A. Jacobson, Z.-G, Gao. Adenosine receptors as therapeutic targets. Nat. Rev. Drug Discov. 5 (2006) 247–264.

[7] S. L. Cheong, S. Federico, G. Venkatesan, A. L. Mandel, Y.-M. Shao, S. Moro, G. Spalluto, G. Pastorin. The A_3 adenosine receptor as multifaceted therapeutic target: pharmacology, medicinal chemistry, and in silico approaches. Med. Res. Rev. 33 (2013) 235–335.

[8] P. A. Borea, K. Varani, F. Vincenzi, P. G. Baraldi, M. A. Tabrizi, S. Merighi, S. Gessi, The A_3 adenosine receptor: history and perspectives. Pharmacol. Rev. 67 (2015) 74–102.

[9] C.N. Wilson, A. Nadeem, D. Spina, R. Brown, C. P. Page, S. J. Mustafa. Adenosine receptors and asthma. Handb. Exp Pharmacol. 193 (2009) 329-362.

[10] F.J.A. Dennissen, M. Anglada-Huguet, A. Sydow, E. Mandelkow, E. M. Mandelkow. Adenosine A_1 receptor antagonist rolofylline alleviates axonopathy caused by human Tau DeltaK280. Proc. Natl. Acad. Sci. U.S.A. 113 (2016) 11597–11602.

[11] S. Li, N. H. Geiger, M. L. Soliman, L. Hui, J. D. Geiger, X. Chen, P. Agostinho. Caffeine, through adenosine A_3 receptor-mediated actions, suppresses amyloid-β protein precursor internalization and amyloid-β generation. J. Alzheimers Dis., 47 (2015) 73–83.

[12] A. Brunschweiger, P. Koch, M. Schlenk, F. Pineda, P. Kuppers, S. Hinz, M. Kose, S. Ullrich, J. Hockemeyer, M. Wiese, J. Heer, C. E. Müller. 8-Benzyltetrahydropyrazino2,1-fpurinediones: water-soluble tricyclic xanthine derivatives as multitarget drugs for neurodegenerative diseases. Chem. Med. Chem. 9 (2014) 1704–1724.

[13] B. Hocher. Adenosine A_1 receptor antagonists in clinical research and development. Kidney Int. 78 (2010) 438-445.

[14] J. R. Teerlink, V. J. Iragui, J. P. Mohr, Carson, P. E.; Hauptman, P. J.; Lovett, D. H.; Miller, A. B.; Pina, I. L.; Thomson, S.; Varosy, P. D. et al. The safety of an adenosine A_1-receptor antagonist, rolofylline, in patients with acute heart failure and renal impairment: findings from PROTECT. Drug Saf. 35 (2012) 233–244.

[15] B. G. Demissei, D. Postmus, L. C. Y. Liu, J. G. Cleland, C. M. O'Connor, M. Metra, P. Ponikowski, J. R. Teerlink, G. Cotter, B. A. Davison, C. Edwards, M. M. Givertz, D. M. Bloomfield, H. C. Dittrich, A. A. Voors, H. L. Hillege. Risk-based evaluation of efficacy of rolofylline in patients hospitalized with acute heart failure - post-hoc analysis of the PROTECT trial. Int. J. Cardiol. 223 (2016) 967–975.

[16] K. A. Jacobson, C. E. Müller, Medicinal chemistry of adenosine, P2Y and P2X receptors. Neuropharmacology 104 (2016) 31–49.

[17] W. J. Geldenhuys, C. J. Van der Schyf. Rationally designed multi-targeted agents against neurodegenerative diseases. Curr. Med. Chem. 20 (2013) 1662–1672.

[18] A. Anighoro, J. Bajorath, G. Rastelli. Polypharmacology: challenges and opportunities in drug discovery. J. Med. Chem. 57 (2014) 7874–7887.

[19] D. Preti, P. G. Baraldi, A. R. Moorman, P. A. Borea, K. Varani. History and perspectives of A_{2A} adenosine receptor antagonists as potential therapeutic agents. Med. Res. Rev. 35 (2015) 790–848.

[20] N. J. Press, R. J. Taylor, J. D. Fullerton, P. Tranter, C. McCarthy, T. H. Keller, L. Brown, R. Cheung, J. Christie, S. Christie J, S. Haberthuer, J. D. Hatto, M. Keenan, M. K. Mercer, N. E. Press, H. Sahri, A. R. Tuffnell, M. Tweed, J. R. Fozard. A new orally bioavailable dual adenosine A_{2B}/A_3 receptor antagonist with therapeutic potential. Bioorg. Med. Chem. Lett. 15 (2005) 3081–3085.

[21] N. Bevan, P. R. Butchers, R. Cousins, J. Coates, E. V. Edgar, V. Morrison, M. J. Sheehan, J. Reeves, D. J. Wilson, Pharmacological characterization and inhibitory effects of (2*R*,3*R*,4*S*,5*R*)-2-(6-amino-2-{(1*S*)-2-hydroxy-1-(phenylmethyl)ethylamino}-9*H*-purin -9-yl)-5-(2-ethyl-2*H*-tetrazol-5-yl)tetrahydro-3,4-furandiol, a novel ligand that demonstrates both adenosine A_{2A} receptor agonist and adenosine A_3 receptor antagonist activity. Eur. J. Pharmacol. 564 (2007) 219–225.

[22] X. Hou, M. S. Majik, K. Kim, Y. Pyee, Y. Lee, V. Alexander, H. J. Chung, H. W. Lee, G. Chandra, J. H. Lee, S. G. Park, W. J. Choi, H. O. Kim, K. Phan, Z. G. Gao, K. A. Jacobson, S. Choi, S. K. Lee, L. S. Jeong. Structure-activity relationships of truncated C2- or C8-substituted adenosine derivatives as dual acting A_{2A} and A_3 adenosine receptor ligands. J. Med. Chem. 55 (2012) 342–356.

[23] B. C. Shook, S. Rassnick, M. C. Osborne, S. Davis, L. Westover, J. Boulet, D. Hall, K. C. Rupert, G. R. Heintzelman, K. Hansen, D. Chakravarty, J. L. Bullington, R. Russell, S. Branum, K. M. Wells, S. Damon, S. Youells, X. Li, D. A. Beauchamp, D. Palmer, M. Reyes, K. Demarest, Y. Tang, K. Rhodes, P. F. Jackson. In vivo characterization of a dual adenosine A_{2A}/A_1 receptor antagonist in animal models of Parkinson's disease. J. Med. Chem. 53 (2010) 8104-8115.

[24] S. Barman, R. A. Baumgartner. Method of reducing intraocular pressure in humans. (2010) WO2010127210 A1.

[25] J. C. Burbiel, W. Ghattas, P. Küppers, M. Köse, S. Lacher, A. M. Herzner, R. S. Kombu, R. R. Akkinepally, J. Hockemeyer, C. E. Müller. 2-Amino[1,2,4]triazolo[1,5-c]quinazolines and derived novel heterocycles: syntheses and structure-activity relationships of potent adenosine receptor antagonists. Chem. Med. Chem. 11 (2016) 2272-2286.

[26] C. E. Müller, K. A. Jacobson. Xanthines as adenosine receptor antagonists. Handb. Exp. Pharmacol. (2011) 151–199.

[27] M. Skouroliakou, F. Bacopoulou, S. L. Markantonis. Caffeine versus theophylline for apnea of prematurity: a randomised controlled trial. J. Paediatr. Child Health 45 (2009) 587–592.

[28] M. W. Alnouri, S. Jepards, A. Casari, C. A. Schiedel, S. Hinz, C. E. Müller, Selectivity is species-dependent: characterization of standard agonists and antagonists at human, rat, and mouse adenosine receptors. Purinergic Signal. 11 (2015) 389–407.

[29] R. K. Y. Cheng, E. Segala, N. Robertson, F. Deflorian, A. S. Dore, J. C. Errey, C. Fiez-Vandal, F. H Marshall, R. M Cooke. Structures of human A_1 and A_{2A} adenosine receptors with xanthines reveal determinants of selectivity. Structure 25 (2017) 1275-1285.

[30] M. T. Slawsky, M. M. Givertz. Rolofylline: a selective adenosine 1 receptor antagonist for the treatment of heart failure. Expert Opin. Pharmaco. ther. 10 (2009) 311-322.

[31] C. E. Müller, T. Scior. Adenosine receptors and their modulators. Pharm. Acta Helv. 68 (1993) 77–111.

[32] S. Moro, Z. G. Gao, K. A. Jacobson, G. Spalluto. Progress in pursuit of therapeutic adenosine receptor antagonists. Med. Res. Rev. 26 (2006) 131–159.

[33] C. B. Mishra, S. K. Barodia, A. Prakash, J. B. Senthil Kumar, P. M. Luthra. Novel 8-(furan-2-yl)-3-substituted thiazolo [5,4-e][1,2,4] triazolo[1,5-c] pyrimidine-2(3H)-thione derivatives as potential adenosine A_{2A} receptor antagonists. Bioorg. Med Chem. 18 (2010) 2491–2500.

[34] P. M. Luthra, C. B. Mishra, P. K. Jha, S. K. Barodia. Synthesis of novel 7-imino-2-thioxo-3,7-dihydro-2H-thiazolo [4,5-d] pyrimidine derivatives as adenosine A_{2A} receptor antagonists. Bioorg. Med. Chem. Lett. 20 (2010) 1214–1218.

[35] C. B. Mishra, D. Sharma, A. Prakash, N. Kumari, N. Kumar, P. M. Luthra, Design and synthesis of (4E)-4-(4-substitutedbenzylideneamino)-3-substituted-2,3-dihydro-2-thioxothiazole-5-carbonitrile as novel A_{2A} receptor antagonists. Bioorg. Med. Chem. 21 (2013) 6077–6083.

[36] B. C. Shook, P. F. Jackson. Adenosine A_{2A} receptor antagonists and Parkinson's disease. ACS Chem. Neurosci. 2 (2011) 555–567.

[37] A. B. Scheiff, S. G. Yerande, A. El-Tayeb, W. Li, G. S. Inamdar,; K. K. Vasu, V. Sudarsanam, C. E. Müller. 2-Amino-5-benzoyl-4-phenylthiazoles: Development of potent and selective adenosine A_1 receptor antagonists. Bioorg. Med. Chem. 18 (2010) 2195–2203.

[38] G. S. Inamdar, A. N. Pandya, H. M. Thakar, V. Sudarsanam, S. Kachler, D. Sabbadin,; S. Moro, K. N. Klotz, K. K. Vasu. New insight into adenosine receptors selectivity derived from a novel series of [5-substituted-4-phenyl-1,3-thiazol-2-yl] benzamides and furamides. Eur. J. Med. Chem. 63 (2013) 924–934.

[39] K. A. Jacobson, A. M. Klutz, D. K. Tosh, A. A. Ivanov, D. Preti, P. G. Baraldi. Medicinal chemistry of the A_3 adenosine receptor: agonists, antagonists, and receptor engineering. Handb. Exp. Pharmacol. 193 (2009) 123–159.

[40] D. H. Pandya, J. A. Sharma, H. B. Jalani, A. N. Pandya, V. Sudarsanam, S. Kachler,; K. N. Klotz, K. K. Vasu. Novel thiazole–thiophene conjugates as adenosine receptor antagonists: Synthesis, biological evaluation and docking studies. Bioorg. Med. Chem. Lett. 25 (2015) 1306–1309.

[41] W. P. Reeves, A. Simmons, J. A. Rudis, T. C. Bothwell. Phase transfer catalysis preparation of acyl isothiocyanates. Synth. Commun. 11 (1981) 781–785.

[42] M. Romero-Ortega, A. Aviles, R. Cruz, A. Fuentes, R. M. Gómez, A. Plata. Synthesis of 4-substituted 2-phenylaminothiazoles from amidines. A convenient route to 4-trichloromethylthiazoles. J. Org. Chem. 65 (2000) 7244–7247.

[43] R. S. Giri, H. M. Thaker, T. Giordano, J. Williams, D. Rogers, V. Sudersanam, K. K. Vasu. Design, synthesis and characterization of novel 2-(2,4-disubstituted-thiazole-5-yl)-3-aryl-3H-quinazoline-4-one derivatives as inhibitors of NF-kappaB and AP-1 mediated transcription activation and as potential anti-inflammatory agents. Eur. J. Med. Chem. 44 (2009) 2184–2189.

[44] R. S. Giri, H. M. Thaker, T. Giordano, J. Williams, D. Rogers, K. K. Vasu, V. Sudarsanam. Design, synthesis and evaluation of novel 2-thiophen-5-yl-3H-quinazolin-4-one analogues as inhibitors of transcription factors NF-κB and AP-1 mediated transcriptional activation: Their possible utilization as anti-inflammatory and anti-cancer agents. Bioorg. Med. Chem. 18 (2010) 2796–2808.

[45] A. Giordano, K. K. Vasu, H. M. Thakar, R. S. Giri, S. G. Yerande, G. S. Inamdar, J. C. Kaila, H. P. Ahmedabad, V. Sudarsanam. Thiazole and thiophene analogues, and their use in treating autoimmune diseases and cancers; US Patents (2009) US20090306073.

[46] S. Vasudevan, G. Anthony, V. K. Kamala, T. M. Hardik, G. S. Rajan, Y. G. Swapnil, I. S. Gajanan. Preparation of thiazoles and thiophenes as inhibitors of transcription factor NF-κB and AP-1 and translation initiation factor eIF-4E for the treatment of inflammation, autoimmune disease and cancer. WO Patents (2007) WO2007118149A2 20071018.

[47] T. Borrmann, S. Hinz, D. C. G. Bertarelli, W. Li, N. C. Florin, A. B. Scheiff, C. E. Müller. 1-alkyl-8-(piperazine-1-sulfonyl)phenylxanthines: development and characterization of adenosine A_{2B} receptor antagonists and a new radioligand with subnanomolar affinity and subtype specificity. J. Med. Chem. 52 (2009) 3994–4006.

[48] K. N. Klotz, M. J. Lohse, U. Schwabe, G. Cristalli, S. Vittori, M. Grifantini,. 2-Chloro-N6-[^{3}H]cyclopentyladenosine ([^{3}H]CCPA) a high affinity agonist radioligand for A_1 adenosine receptors. Naunyn-Schmiedeberg's Arch. Pharmacol. 340 (1989) 679–683.

[49] C. E. Müller, J. Maurinsh, R. Sauer. Binding of [^{3}H]MSX-2 (3-(3-hydroxypropyl)-7-methyl-8-(*m*-methoxystyryl)-1-propargylxanthine) to rat striatal membranes-a new, selective antagonist radioligand for A_{2A} adenosine receptors. Eur. J. Pharm. Sci. 10 (2000) 259–265.

[50] C. E. Müller, M. Diekmann, M. Thorand, V. Ozola, [^{3}H]8-Ethyl-4-methyl-2-phenyl-[8R]-4,5,7,8-tetrahydro-1H-imidazo[2,1-i]-purin-5-one ([^{3}H]PSB-11), a novel high-affinity antagonist radioligand for human A_3 adenosine receptors. Bioorg. Med. Chem. lett. 12 (2002) 501–503.

[51] S. Kehraus, S. Gorzalka, C. Hallmen, J. Iqbal, C. E. Müller, A. D. Wright, M. Wiese, G. M. König. Novel amino acid derived natural products from the ascidian Atriolum robustum: identification and pharmacological characterization of a unique adenosine derivative. J. Med. Chem. 47 (2004) 2243–2255.

[52] H. von der Leyen, W. Schmitz, H. Scholz, J. Scholz, M. J. Lohse, U. Schwabe. Effects of 1,3-dipropyl-8-cyclopentylxanthine (DPCPX), a highly selective adenosine receptor antagonist, on force of contraction in guinea-pig atrial and ventricular cardiac preparations. Naunyn Schmiedebergs Arch. Pharmacol. 340 (1989) 204-209.

[53] T.J Searl, E. M. Silinsky. Evidence for constitutively active adenosine receptors at mammalian motor nerve endings. Eur. J. Pharmacol. 685 (2012) 38–41.

[54] W. He, T. Wilder, B. N. Cronstein. Rolofylline, an adenosine A_1 receptor antagonist, inhibits osteoclast differentiation as an inverse agonist. Br. J. Pharmacol. 170 (2013) 1167–1176.

[55] E. Segala, D. Guo, R. K. Cheng, A. Bortolato, F. Deflorian, A. S. Dore, J. C. Errey,; L. H. Heitman, I. J. AP, F. H. Marshall, R. M, Cooke . Controlling the dissociation of ligands from the adenosine A_{2A} receptor through modulation of salt bridge strength. J. Med. Chem. 59 (2016) 6470-6479.

[56] Yan, L.; Müller, C. E. Preparation, properties, reactions, and adenosine receptor affinities of sulfophenylxanthine nitrophenyl esters: toward the development of sulfonic acid prodrugs with peroral bioavailability. J. Med. Chem. 47 (2004) 1031–1043.

[57] Bulicz, J.; Bertarelli, D. C. G.; Baumert, D.; Fülle, F.; Müller, C. E.; Heber, D. Synthesis and pharmacology of pyrido[2,3-d]pyrimidinediones bearing polar substituents as adenosine receptor antagonists. Bioorg. Med. Chem. 14 (2006) 2837–2849.

[58] C. Nordstedt, B. B. Fredholm. A modification of a protein-binding method for rapid quantification of cAMP in cell-culture supernatants and body fluid. Anal. Biochem. 189 (1990) 231–234.

[59] A. C. Schiedel, S. Hinz, D. Thimm, F. Sherbiny, T. Borrmann, A. Maass, C. E. Müller. The four cysteine residues in the second extracellular loop of the human adenosine A_{2B} receptor: role in ligand binding and receptor function. Biochem. Pharmacol. 82 (2011) 389–399.

[60] W. Liu, E. Chun, A. A. Thompson, P. Chubukov, F. Xu, V. Katritch, G. W. Han, C. B. Roth, Heitman, L. H.; IJzerman, A. P. Cherezov, V.; Stevens, R. C. Structural basis for allosteric regulation of GPCRs by sodium ions. Science 337 (2012) 232–236.

[61] A. Sali, T. L. Blundell. Comparative protein modelling by satisfaction of spatial restraints. J. Mol. Biol. 234 (1993) 779–815.

[62] F. Sievers, A. Wilm, D. Dineen, T. J. Gibson, K. Karplus, W. Li, R. Lopez, H. McWilliam, M. Remmert, J. Söding, J. D. Thompson, D. G. Higgins. Fast, scalable generation of high-quality protein multiple sequence alignments using Clustal Omega. Mol. Sys. Biol. 7 (2011) 539.

[63] M. Y. Shen, A. Sali. Statistical potential for assessment and prediction of protein structures. Protein Sci. 15 (2006) 2507–2524.

[64] Molecular operating environment (MOE 2018.01): chemical computing group: Montreal, Quebec, Canada. (2018).

[65] Wiederstein, M.; Sippl, M. J. ProSA-web: interactive web service for the recognition of errors in three-dimensional structures of proteins. Nuc. Acids Res. 2007, W407-10.

[66] G. N. Ramachandran, C. Ramakrishnan, V. Sasisekharan. Stereochemistry of polypeptide chain configurations. J. Mol. Biol. 7 (1963) 95–99.

[67] G. M. Morris, R. Huey, W. Lindstrom, M. F. Sanner, R. K. Belew, D. S. Goodsell, A. J. Olson. Auto Dock4 and Auto Dock Tools4: automated docking with selective receptor flexibility. J. Comp. Chem. 30 (2009) 2785–2791.

[68] M. F. Sanner. Python: a programming language for software integration and development. J. Mol. Graph. Model. 17 (1999) 57–61.

[69] Namasivayam, V., Gunther, R. pso@autodock: a fast flexible molecular docking program based on Swarm intelligence. Chem. Biol. Drug Des. 70 (2007) 475–484.

[70] J. Lee, X. Cheng, J. M. Swails, M. S. Yeom, P. K. Eastman, J. A. Lemkul, S. Wei, J. Buckner, J. C. Jeong, Y. Qi, S. Jo, V. S. Pande, D. A. Case, CL. 3rd. Brooks, AD. Jr. Mackerel, J.B. Klauda, W. Im, CHARMM-GUI input generator for NAMD, GROMACS, AMBER, OpenMM, and CHARMM/OpenMM simulations using the CHARMM36 additive force field. J. Chem. Theory Comput. 12 (2016) 405-413.

[71] S. Jo, T. Kim, V. G. Iyer, W. Im. CHARMM-GUI: a web-based graphical user interface for CHARMM. J. Comput. Chem. 29 (2008), 1859-1865.

[72] W. L. Jorgensen, J. Chandrasekhar, J.D. Madura, R.W. Impey, M. L. Klein, Comparison of simple potential functions for simulating liquid water. J. Chem. Phys. 79 (1983) 926-935.

[73] K. Vanommeslaeghe, E. Hatcher, C. Acharya, S. Kundu, S. Zhong, J. Shim, E. Darian, O. Guvench, P. Lopes, I. Vorobyov, AD. Jr. Mackerell. CHARMM general force field: A force field for drug-like molecules compatible with the CHARMM all-atom additive biological force fields. J. Comput. Chem. 31 (2010) 671-690.

[74] J. Huang, S. Rauscher, G. Nawrocki, T. Ran, M. Feig, B. L. de Groot, H. Grubmuller, A. D. MacKerell, Jr. CHARMM36m: an improved force field for folded and intrinsically disordered proteins. Nat. Methods 14 (2017) 71-73.

[75] J. C. Phillips, R. Braun, W. Wang, J. Gumbart, E. Tajkhorshid, E. Villa, C. Chipot, R. D. Skeel, L. Kale, K. Schulten, Scalable molecular dynamics with NAMD. J. Comput. Chem. 26 (2005) 1781-802.

[76] T. Darden, D. Your, L. Pedersen. Particle mesh Ewald. An N log (N) method for Ewald sums in large systems. J. Chem. Phys. 98 (1993) 10089-10092.

[77] M. J. Harvey, G. Giupponi, G. D. Fabritiis. ACEMD: accelerating biomolecular dynamics in the microsecond time scale. J. Chem. Theory Comput. 5 (2009) 1632-1639.

[78] W. Humphrey, A. Dalke, K. Schulten. VMD: visual molecular dynamics. J. Mol. Graph. 14 (1996) 33-8, 27-8.

Table of Contents Graphic

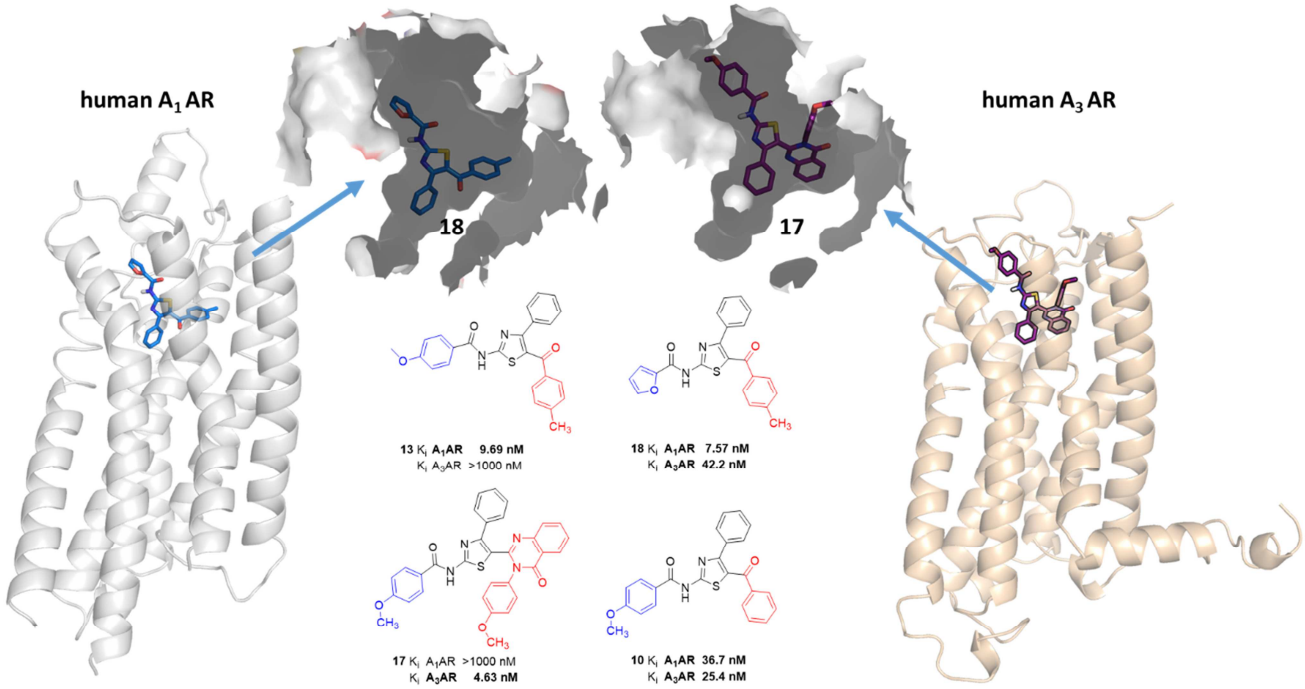

Highlights

- ✓ 2-Amino-4-phenylthiazole derivatives were designed as A_1-, A_3-, or dual A_1/A_3-adenosine receptor (AR) antagonists.
- ✓ Selective A_1 AR antagonists with inverse agonistic activity showing (sub)nanomolar potency were obtained.
- ✓ Selective A_3 AR antagonists showing nanomolar potency were identified.
- ✓ Species differences (human / rat) were observed for both AR subtypes.
- ✓ Potent dual antagonists for A_1 and A_3 AR were developed as potential therapeutics for treating kidney failure, pulmonary diseases, and Alzheimer's disease.